Asia Pac. J. Math. 2026 **13**:117

BIVARIATE FLOOD FREQUENCY ANALYSIS USING AN EXTENDED RLUF-TYPE COPULA: APPLICATION TO REGION XI, PHILIPPINES

JOE VINCENT B. DELUAO

Department of Mathematics, University of Southeastern Philippines, Philippines
joe.deluao@usep.edu.ph

Received Apr. 9, 2026

Abstract. Flood events are inherently multivariate phenomena defined by the complex stochastic interaction of flood duration (D), severity (S), and peak (P). Traditional univariate frequency analyses often overlook these interdependencies, leading to biased risk assessments in hydraulic design. This study introduces an extended RLUF-type copula framework to model the joint dependence structure of these characteristics across Region XI, Philippines. Optimal marginal distributions were rigorously identified via the Anderson–Darling test and information criteria, revealing that the Lomax distribution consistently represents duration, while the Generalized Gamma (and Fatigue Life in specific rugged topographies) and Beta Prime distributions best capture peak and severity, respectively. Dependence modeling integrated Archimedean and elliptical families (specifically BB1, BB7, and Clayton architectures) to capture the intricate tail dependencies and asymmetric associations inherent in the region's hydrological regime. The results demonstrate that the extended RLUF-type copula significantly outperforms conventional models in representing nonlinear dependencies. Spatial hazard mapping via joint return periods (T_{AND}) identifies Davao de Oro and Davao Oriental as high-risk hotspots for compound extremes $(S > 2, P > 2)$, with recurrence intervals as frequent as 2.6 to 4.8 years. Furthermore, mountainous provinces exhibit a non-negligible risk for prolonged, high-severity inundations $(D > 6)$. This framework provides a mathematically versatile approach for multivariate flood frequency analysis, offering critical insights for hydrological infrastructure planning and the enhancement of regional disaster risk reduction strategies.
2020 Mathematics Subject Classification: Primary 62E15; Secondary 62F10, 62P12.
Key words and phrases. copula modeling; RLUF-type copula; flood frequency analysis; bivariate return period; hydrological extremes; multivariate analysis; flood risk assessment.

1. Introduction

Flooding persists as one of the most catastrophic natural hazards globally, precipitating profound socio-economic disruptions, infrastructure degradation, and mortality, especially within the climatologically sensitive regions of Southeast Asia. In the Philippines, the intensification of extreme precipitation,

DOI: 10.28924/APJM/13-117

modulated by both anthropogenic land-use changes and heightened climate variability, has exacerbated flood vulnerability, particularly in the socio-economically vital Region XI. Given these escalating threats, the precise characterization of flood regimes is paramount for resilient hydraulic engineering, sustainable water resource management, and robust disaster risk reduction (DRR) strategies.

Conventional Flood Frequency Analysis (FFA) has historically relied upon univariate frameworks, typically focusing on peak discharge in isolation. While such approaches are computationally parsimonious, they inherently fail to account for the multivariate stochasticity of flood events. Floods are fundamentally characterized by the synergistic interaction of multiple variables, most notably duration (D), severity (S), and peak intensity (P). Neglecting the cross-correlation and dependency structures between these attributes can lead to systematic underestimations of hydrological risk, particularly during extreme return periods [29,39]. Consequently, Multivariate Flood Frequency Analysis (MFFA) has emerged as a critical paradigm for capturing the joint probabilistic behavior of these interdependent phenomena.

Copula theory has revolutionized MFFA by providing a flexible mathematical apparatus that decouples marginal distributions from their joint dependence structure [26]. This modularity is uniquely suited for hydrological data, where variables often exhibit heterogeneous marginal behaviors. While traditional Archimedean and elliptical copulas, such as the Gumbel, Clayton, and Student-t families, have been employed to model these relationships, they often struggle to simultaneously accommodate complex, nonlinear, and asymmetric tail dependencies [10,14].

To overcome these structural limitations, recent developments in vine and hierarchical copula constructions have sought to enhance model flexibility [1,5]. Among these, the extended RLUF copula represents a significant advancement. The extended RLUF-type copula [8,16] allows for the synthesis of multiple base copulas, thereby providing a more versatile architecture for representing joint behaviors that exhibit both upper and lower tail dependencies.

Building upon these theoretical foundations, this study proposes an *extended RLUF-type copula* framework for bivariate flood analysis, incorporating a suite of candidate models including Student-t, Clayton, Gumbel, BB1, and BB7 copulas. Utilizing Standardized Precipitation Index (SPI)-derived flood characteristics, the marginal distributions are rigorously identified through the Anderson–Darling (AD) test, Root Mean Square Error (RMSE), and Information Criteria (AIC and BIC). The performance of the RLUF-based model is subsequently benchmarked against conventional copula configurations.

The primary objectives of this research are threefold: (1) to develop a high-fidelity, flexible copula framework capable of capturing multifaceted dependence structures; (2) to quantitatively evaluate the goodness-of-fit and tail-behavior representation of the RLUF-type model relative to standard methodologies; and (3) to derive spatially explicit joint return periods for Region XI, Philippines. By providing a more nuanced estimation of simultaneous flood risks, this study offers a robust analytical tool for climate adaptation planning and hydrological safety assessment in high-risk tropical catchments.

2. Methodology

2.1. **Standardized Precipitation Index (SPI).** Monthly precipitation datasets spanning a 30-year period (1995–2025) were retrieved from the NASA Prediction of Worldwide Energy Resources (POWER) Data Access Viewer [25]. These data were aggregated at a monthly resolution for designated locations across Region XI, Philippines. To account for inherent seasonality and ensure statistical homogeneity, the time series was partitioned into twelve monthly sub-series, adhering to the SPI framework established by McKee et al. [22,23]. A one-month timescale (SPI-1) was adopted to facilitate the identification of high-frequency variability and transient hydrometeorological extremes.

The precipitation data for each sub-series were modeled using a two-parameter gamma distribution, which is theoretically robust for characterizing positively skewed hydrological variables [35]. The probability density function $g(x)$ is defined as:

$$g(x) = \frac{1}{\beta^{\alpha}\Gamma(\alpha)} x^{\alpha-1} e^{-x/\beta}, \quad \text{for } x > 0 \tag{1}$$

where α and β represent the shape and scale parameters, respectively. These parameters were estimated via the Maximum Likelihood Estimation (MLE) method:

$$\hat{\alpha} = \frac{1}{4A}\left(1 + \sqrt{1 + \frac{4A}{3}}\right), \quad \hat{\beta} = \frac{\bar{x}}{\hat{\alpha}} \tag{2}$$

where A is given by:

$$A = \ln(\bar{x}) - \frac{1}{n}\sum_{i=1}^{n} \ln(x_i) \tag{3}$$

Since the gamma distribution is undefined for zero precipitation, a mixed distribution was employed to incorporate the probability of zero events ($q = m/n$):

$$H(x) = q + (1-q)G(x) \tag{4}$$

where $G(x)$ denotes the cumulative distribution function (CDF) of the gamma model. The final SPI values were derived by transforming the cumulative probability $H(x)$ into a standard normal variate with zero mean and unit variance:

$$\text{SPI} = \Phi^{-1}(H(x)) \tag{5}$$

where Φ^{-1} is the inverse standard normal cumulative distribution function.

The resulting SPI values were interpreted according to the World Meteorological Organization (WMO) standards [37], as summarized in Table 1. This standardized approach ensures that anomalies are comparable across different spatial and temporal scales within the study region.

TABLE 1. Classification of SPI values for wet and dry conditions (adapted from McKee et al. [22] and WMO [37]).

SPI Range	Category
SPI ≥ 2.00	Extremely wet
$1.50 \leq$ SPI < 2.00	Very wet
$1.00 \leq$ SPI < 1.50	Moderately wet
$-1.00 <$ SPI < 1.00	Near normal
$-1.50 <$ SPI ≤ -1.00	Moderately dry
$-2.00 <$ SPI ≤ -1.50	Severely dry
SPI ≤ -2.00	Extremely dry

2.2. **Flood-Event Variable Extraction via Run Theory.** Flood-event characteristics were extracted from the monthly SPI-1 series using a threshold-based *run theory* framework [38]. Within this context, flood events are conceptualized as "wet runs", maximal contiguous periods of positive SPI-1 values that exceed a prescribed intensity threshold at least once. This approach leverages the symmetric applicability of the SPI to both moisture deficits and surpluses [31,37]. For each identified event, three fundamental descriptors were derived: **flood duration** (D), **flood peak** (P), and **flood severity** (S), providing the multivariate basis for subsequent dependence modeling [9,33].

While flood processes are physically complex, these event-based metrics serve as primary stochastic descriptors of flood behavior [24]. In this study, these variables are derived from the SPI-1 series as a meteorological proxy, representing precipitation-driven "wet spells" associated with elevated flood *potential* rather than direct riverine discharge [31].

Let $\{z_t\}_{t=1}^{N}$ denote the SPI-1 time series and $T > 0$ represent the critical wetness threshold (fixed at $T = 1.0$ for moderately wet conditions). A wet run $\mathcal{R}_e$ is defined as a maximal sequence where $z_t > 0$. A flood event is formally identified if:

$$\max_{t \in \mathcal{R}_e} z_t \geq T \tag{6}$$

For each discrete event e, the following hydrological metrics were quantified:

Flood Duration (D_e)**:** The temporal span of the wet run, defined as the number of months between the start and end of the event:

$$D_e = |\mathcal{R}_e| = t_{end}^{(e)} - t_{start}^{(e)} + 1 \tag{7}$$

Flood Peak (P_e)**:** The maximum standardized anomaly recorded during the event, representing the highest wetness intensity:

$$P_e = \max_{t \in \mathcal{R}_e} z_t \tag{8}$$

Flood Severity (S_e)**:** The cumulative water surplus relative to the threshold T, representing the total event magnitude:

$$S_e(T) = \sum_{t \in \mathcal{R}_e} (z_t - T)_+ \tag{9}$$

These formulations adhere to the run-sum representation of hydrological magnitudes [38] and are consistent with established Peaks-Over-Threshold (POT) guidelines [18,33].

2.2.1. *Algorithmic Implementation.* The extraction procedure was executed via a five-stage algorithmic sequence: (i) identification of all positive SPI-1 tranches $(z_t > 0)$; (ii) segmentation of these tranches into contiguous temporal runs; (iii) application of the truncation level $T = 1.0$ to filter significant events; (iv) computation of the triplet (D_e, P_e, S_e) for each qualified run; and (v) structural organization of the resulting multivariate dataset for copula fitting. This systematic approach ensures the objective identification of precipitation-driven extremes across the diverse climatic sub-regions of Region XI.

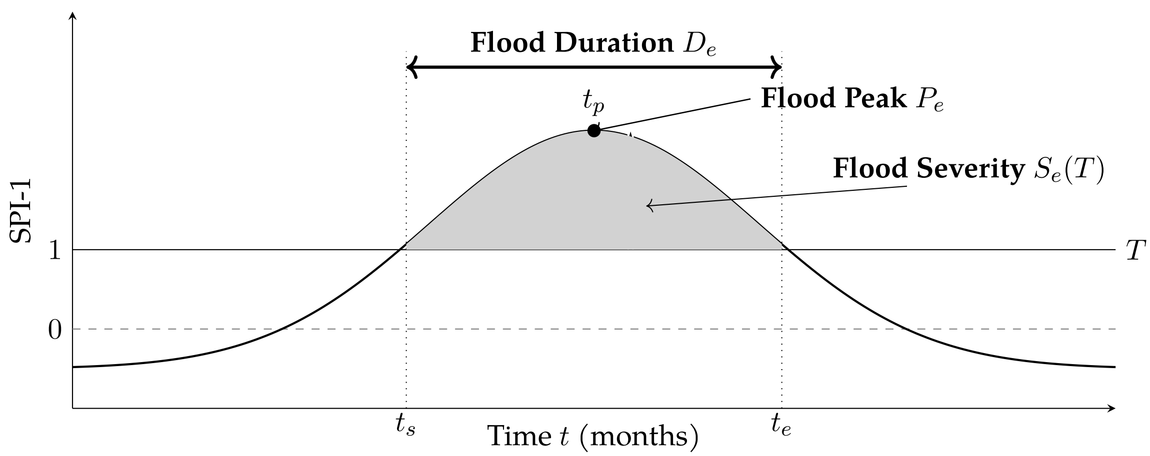

Figure 1. Schematic representation of SPI-based flood characteristics. Flood severity $S_e(T)$ denotes the cumulative exceedance above the threshold $T = 1$.

2.3. **The Data Set and Regional Characteristics.** This section presents the descriptive statistics of flood duration (D), severity (S), and peak (P) across the provinces of Region XI, Philippines. Quantifying central tendency, dispersion, and higher-order moments—specifically skewness and kurtosis—is a prerequisite for assessing the asymmetry and tail behavior that inform the selection of marginal distributions and RLUF-type copula models.

Note: Due to the spatial resolution of the NASA POWER dataset $(0.5^\circ \times 0.5^\circ)$, *certain contiguous administrative areas, such as Davao City and Davao del Sur, correspond to the same primary grid nodes. Consequently, the descriptive statistics for these specific locations are identical, reflecting the regional homogeneity of the satellite-derived precipitation anomalies at this scale.*

TABLE 2. Descriptive statistics of flood duration (D) across Region XI.

Location	N	Mean	SD	Min	Max	Skew	Kurt
Davao City	43	1.21	0.74	1.00	5.00	4.04	17.40
Davao de Oro	46	1.22	0.51	1.00	3.00	2.38	5.07
Davao del Norte	42	1.40	0.86	1.00	4.00	2.02	2.94
Davao del Sur	43	1.21	0.74	1.00	5.00	4.04	17.40
Davao Occidental	40	1.18	0.45	1.00	3.00	2.64	6.87
Davao Oriental	49	1.20	0.50	1.00	3.00	2.49	5.66

As summarized in Table 2, flood durations in the region are typically short, with mean values ranging from 1.18 to 1.40 months. However, the high standard deviation in Davao del Norte (0.86) suggests significant intra-regional variability. Notably, all locations exhibit strong positive skewness $(\gamma > 2.0)$ and pronounced leptokurtosis, particularly in the Davao City/Sur grid $(\kappa = 17.40)$. These metrics indicate a dominance of short-lived events punctuated by rare, extremely persistent wet spells.

TABLE 3. Descriptive statistics of flood severity (S) across Region XI.

Location	N	Mean	SD	Min	Max	Skew	Kurt
Davao City	43	0.66	0.74	0.03	3.31	2.11	4.49
Davao de Oro	46	0.53	0.49	0.00	2.63	2.09	6.78
Davao del Norte	42	0.59	0.58	0.00	2.41	1.56	2.42
Davao del Sur	43	0.66	0.74	0.03	3.31	2.11	4.49
Davao Occidental	40	0.71	0.62	0.00	2.78	1.54	2.82
Davao Oriental	49	0.55	0.57	0.00	2.58	1.91	4.08

Flood severity (S), which quantifies the cumulative standardized water surplus, exhibits mean values between 0.53 and 0.71 (Table 3). The skewness coefficients $(1.54–2.11)$ suggest that while the majority of events are of low to moderate severity, the distribution is heavily right-weighted. The positive kurtosis values confirm a leptokurtic behavior across all stations, necessitating the use of distributions capable of capturing heavy-tailed characteristics.

Table 4. Descriptive statistics of flood peak (P) across Region XI.

Location	N	Mean	SD	Min	Max	Skew	Kurt
Davao City	43	1.55	0.52	1.03	3.76	2.15	6.45
Davao de Oro	46	1.47	0.35	1.00	2.38	0.83	0.17
Davao del Norte	42	1.48	0.38	1.00	2.39	0.62	-0.62
Davao del Sur	43	1.55	0.52	1.03	3.76	2.15	6.45
Davao Occidental	40	1.64	0.52	1.00	3.78	1.82	5.98
Davao Oriental	49	1.48	0.47	1.00	3.39	1.90	4.72

Table 4 illustrates consistent flood peak intensities, with regional means centered around 1.50. While Davao del Norte exhibits a slightly negative kurtosis (-0.62), most provinces, particularly Davao City and Davao Occidental, demonstrate significant positive skewness and elevated kurtosis. This divergence implies that peak intensities in specific locales are more susceptible to extreme outliers.

Overall, the non-normal characteristics, pronounced asymmetry, and heavy-tailed nature of the triplets (D, S, P) justify the transition to a flexible RLUF-type copula framework, as conventional Gaussian-based multivariate models would likely underestimate the risk associated with these extreme joint dependencies.

2.4. **Candidate Univariate Marginal Distributions.** The descriptive analysis presented in the preceding section confirms that flood duration (D), peak (P), and severity (S) exhibit pronounced positive skewness and leptokurtic behavior across all stations. These characteristics reflect the inherently heavy-tailed nature of hydrometeorological extremes in tropical contexts. Consequently, a suite of flexible, non-negative parametric distributions was selected for marginal modeling, chosen for their theoretical robustness and established efficacy in multivariate hydrological frequency analysis.

Flood Duration (D): Given the presence of prolonged wet runs, duration was modeled using the Lomax (Pareto Type II), Log-gamma, Log-logistic (Fisk), and Inverse Gaussian distributions. These models are particularly adept at capturing high-frequency short-duration events while maintaining the mathematical flexibility to represent heavy-tailed extremes [4,7,19,32].

Flood Peak (P): To characterize maximum intensity anomalies, the three-parameter Birnbaum–Saunders (Fatigue Life), Johnson SB, Inverse Gaussian, Generalized Gamma, and Lognormal distributions were evaluated. The multi-parameter configurations of these distributions facilitate a more nuanced representation of the location, scale, and shape parameters, which is critical for modeling the extremal behavior of standardized anomalies [13,15,20,21,34].

Flood Severity (S): Representing the cumulative magnitude of the event, severity was modeled via the Inverse Gaussian, Lognormal, Pearson Type V (Inverse Gamma), Pearson Type VI (Beta Prime), and

Log-logistic distributions. These families are well-regarded for their ability to model the right-skewed variability and cumulative stochastic processes typical of flood volumes and magnitudes [6,17,21,32,36].

The selection of these specific distributions ensures that the subsequent goodness-of-fit procedures, utilizing the Anderson–Darling (AD) test and information criteria (AIC/BIC), are conducted within a statistically robust and hydrologically relevant framework.

2.5. **Copula Modeling and Dependence Structures.** Following the identification of the optimal univariate marginal distributions, the multivariate dependence structure among flood duration, peak, and severity was characterized using copula functions. This two-stage inference framework facilitates a versatile modeling approach by decoupling the marginal behavior from the joint dependence structure.

A copula is a multivariate cumulative distribution function defined on the unit hypercube $[0,1]^d$ with uniform marginals [26]. According to Sklar's theorem, for any pair of continuous random variables X and Y with marginal distributions F_X and F_Y, their joint distribution F_{XY} can be uniquely represented as:

$$F_{XY}(x,y) = C(F_X(x), F_Y(y)) = C(u,v) \tag{10}$$

where $u = F_X(x)$ and $v = F_Y(y)$ are the probability integral transforms, and C is the copula function that captures the dependency characteristics.

This study utilizes the RLUF-type copula proposed by [8], which originates from the RLUF family [27]. The standard RLUF construction is defined as:

$$C(u,v) = uv + \theta f(u)g(v) \tag{11}$$

where f and g are absolutely continuous functions satisfying the boundary conditions $f(0) = f(1) = g(0) = g(1) = 0$. The parameter θ is constrained within bounds that ensure the resulting function remains a valid copula.

A significant limitation of the baseline RLUF-type copula is its inherent tail independence, which restricts its utility in modeling the simultaneous occurrence of extreme hydrological events. To circumvent this, a generalized RLUF formulation was adopted, which incorporates a baseline copula $C^*(u,v)$ [12]:

$$C(u,v) = C^*(u,v) + \theta f(u)g(v) \tag{12}$$

By integrating a baseline copula, the model inherits the tail dependence properties of C^*, providing a mechanism to account for extremal co-movements.

To ensure a comprehensive evaluation of the dependence structure, the baseline models evaluated in this study include the Student-t, Clayton, Gumbel, BB1, and BB7 copulas. These families are selected for their ability to capture diverse dependence patterns, including symmetric, lower-tail, and upper-tail associations. These baseline models are integrated within the generalized RLUF framework to provide a flexible and robust representation of the complex, nonlinear dependencies observed between flood characteristics in Region XI.

2.6. **Model Selection and Goodness-of-Fit Criteria.** The identification of the optimal modeling framework was conducted through a hierarchical evaluation process using a suite of complementary goodness-of-fit (GOF) and selection criteria, including the Anderson–Darling (AD) test, Root Mean Square Error (RMSE), Akaike Information Criterion (AIC), and Bayesian Information Criterion (BIC). This approach ensures a statistically robust balance between model fidelity and parsimonious parameterization [11].

For the univariate marginal distributions, a stringent two-stage selection protocol was implemented. First, the AD test was utilized as a primary screening mechanism due to its heightened sensitivity to the tails of the distribution, which is essential for characterizing hydrological extremes [3]. The test statistic is defined as:

$$A^2 = -n - \frac{1}{n}\sum_{i=1}^{n}(2i-1)\left[\ln F(x_{(i)}) + \ln\left(1 - F(x_{(n+1-i)})\right)\right] \tag{13}$$

where F represents the cumulative distribution function (CDF) of the fitted model and $x_{(i)}$ denotes the ordered sample data. Statistical priority was given exclusively to models that satisfied the condition of $p > 0.05$, ensuring that the theoretical distribution is statistically indistinguishable from the empirical data. Among the candidate models that passed the AD test, the optimal distribution was determined based on the minimum values of the AIC and BIC.

For the copula models, including the Student-t, Clayton, Gumbel, BB1, BB7, and their generalized RLUF-type extensions, selection was primarily guided by the AIC and BIC:

$$\text{AIC} = -2\ell(\hat{\theta}) + 2k \tag{14}$$

$$\text{BIC} = -2\ell(\hat{\theta}) + k\ln(n) \tag{15}$$

where $\ell(\hat{\theta})$ is the maximized log-likelihood and k is the number of parameters and n is the number of observation. While RMSE was calculated to quantify the localized discrepancy between the empirical and theoretical copulas, it was not utilized as the primary selection metric. This decision is based on the study's objective to estimate joint return periods, which requires a model with superior predictive capability across the entire probability space rather than one that merely minimizes residuals for the observed dataset.

The AIC and BIC provide a more rigorous basis for return period prediction by penalizing over-parameterization, thereby reducing the likelihood of model over-fitting. This ensures that the selected copula captures the underlying stochastic dependence structure efficiently, providing more reliable estimates for extreme joint probabilities that may lie outside the range of historical observations [2,30].

Consequently, the model exhibiting the lowest information-theoretic indices was selected as the superior architecture for multivariate risk assessment.

2.7. **Joint Return Periods.** The return period serves as a foundational metric for quantifying the expected recurrence interval of extreme events. Traditional univariate approaches fail to represent the synergistic risk posed by interdependent variables, necessitating a multivariate framework predicated on copula theory to integrate the dependence structures of flood duration, severity, and peak.

In this study, flood hazard is characterized through the joint (AND) return period (T_{AND}), which represents the expected interval where both variables X and Y simultaneously exceed their respective thresholds x and y [28]:

$$T_{\text{AND}} = \frac{1}{P(X > x, Y > y)} = \frac{1}{1 - F_X(x) - F_Y(y) + C(F_X(x), F_Y(y))} \tag{16}$$

where $F_X(x)$ and $F_Y(y)$ are the marginal cumulative distributions and $C(\cdot,\cdot)$ is the fitted copula.

The T_{AND} metric is critical for the design of high-stakes hydraulic infrastructure, where the compound occurrence of multiple extreme characteristics poses the greatest threat to structural integrity [29]. Accordingly, the spatial hazard mapping in this research is focused exclusively on the T_{AND} framework, as it provides a rigorous assessment of compound extremes. Utilizing the generalized RLUF-type copula ensures these hazard profiles account for the complex tail dependencies inherent in the tropical hydrological regimes of the region.

3. Results and Discussion

3.1. **Selection of Marginal Distribution.** The specification of marginal distributions is critical for robust joint risk estimation. Candidate models were fitted using maximum likelihood and screened via a hierarchical protocol: models were first required to satisfy the Anderson–Darling (AD) threshold ($p > 0.05$), with the optimal distribution then selected based on minimum AIC and BIC.

As detailed in Table 5, the Lomax (Pareto Type II) distribution emerged as the superior model for flood duration across all locations. While the Fisk distribution occasionally yielded a lower RMSE, it was rejected in several provinces due to inferior p-values. Furthermore, the inverse Gaussian and log-gamma distributions were systematically excluded for failing the 5% significance threshold ($p < 0.05$). Graphical diagnostics (Figure 2) confirm that the Lomax distribution most effectively captures the heavy-tailed behavior and right-skewness observed in the regional data.

Table 5. Comparative Evaluation of Probability Distributions and Parameter Estimates for Regional Flood Duration Modeling

Location	Distribution	Parameter	AD Stat	AD p-value	RMSE	AIC	BIC
Davao City	Inverse Gaussian	Shape(μ): 189.7503, Scale: 0.0011	16.7814	0.0000	0.2980	-379.243	-373.959
	Fisk	Shape(c): 1.4143, Scale: 0.0012	14.5183	0.0100	0.2501	-363.750	-358.467
	Lomax	Shape(c): 0.6896, Scale: 0.0008	12.8431	0.7800	0.2527	-362.663	-357.379
	Gamma	Shape(α): 0.1635, Rate(β): 0.7775	14.6484	0.4267	0.2788	-273.088	-267.804
	Log-gamma	Shape(c): 1.6196, Scale: 1.4737	13.4241	0.0000	0.2633	137.771	143.055
Davao de Oro	Inverse Gaussian	Shape(μ): 179.4434, Scale: 0.0012	14.6681	0.0000	0.2590	-338.041	-332.555
	Fisk	Shape(c): 0.8196, Scale: 0.0017	12.9854	0.0967	0.2211	-302.915	-297.429
	Lomax	Shape(c): 0.4811, Scale: 0.0006	11.2921	0.5600	0.2257	-318.925	-313.439
	Gamma	Shape(α): 0.1800, Rate(β): 0.8243	12.3852	0.3900	0.2443	-251.982	-246.496
	Log-gamma	Shape(c): 1.7518, Scale: 0.8775	11.2713	0.0000	0.2307	98.899	104.385
Davao del Norte	Inverse Gaussian	Shape(μ): 317.8676, Scale: 0.0013	12.7633	0.0000	0.2428	-263.878	-258.665
	Fisk	Shape(c): 0.6438, Scale: 0.0023	10.5110	0.2100	0.2088	-229.463	-224.250
	Lomax	Shape(c): 0.3968, Scale: 0.0006	9.4079	0.4833	0.2140	-248.703	-243.490
	Gamma	Shape(α): 0.1710, Rate(β): 0.4215	9.9324	0.4133	0.2277	-194.996	-189.783
	Log-gamma	Shape(c): 1.8043, Scale: 1.4079	9.3510	0.0000	0.2190	130.302	135.515
Davao del Sur	Inverse Gaussian	Shape(μ): 189.7503, Scale: 0.0011	16.7814	0.0000	0.2980	-379.243	-373.959
	Fisk	Shape(c): 1.4143, Scale: 0.0012	14.5183	0.0100	0.2501	-363.750	-358.467
	Lomax	Shape(c): 0.6896, Scale: 0.0008	12.8431	0.7800	0.2527	-362.663	-357.379
	Gamma	Shape(α): 0.1635, Rate(β): 0.7775	14.6484	0.4267	0.2788	-273.088	-267.804
	Log-gamma	Shape(c): 1.6196, Scale: 1.4737	13.4241	0.0000	0.2633	137.771	143.055
Davao Occidental	Inverse Gaussian	Shape(μ): 148.6242, Scale: 0.0012	13.4101	0.0000	0.2705	-313.432	-308.366
	Fisk	Shape(c): 0.9525, Scale: 0.0015	12.0305	0.0633	0.2291	-285.967	-280.901
	Lomax	Shape(c): 0.5363, Scale: 0.0007	10.3929	0.6567	0.2335	-296.532	-291.465
	Gamma	Shape(α): 0.1815, Rate(β): 1.0310	11.5957	0.4100	0.2550	-233.120	-228.053
	Log-gamma	Shape(c): 1.7198, Scale: 0.7853	10.4175	0.0000	0.2404	77.935	83.001
Davao Oriental	Inverse Gaussian	Shape(μ): 170.6282, Scale: 0.0012	15.9562	0.0000	0.2634	-370.950	-365.275
	Fisk	Shape(c): 0.8704, Scale: 0.0016	14.2218	0.0933	0.2246	-334.784	-329.109
	Lomax	Shape(c): 0.5024, Scale: 0.0007	12.3339	0.6367	0.2290	-350.354	-344.678
	Gamma	Shape(α): 0.1796, Rate(β): 0.8756	13.6083	0.3533	0.2485	-275.976	-270.301
	Log-gamma	Shape(c): 1.7369, Scale: 0.8637	12.3762	0.0000	0.2346	103.547	109.222

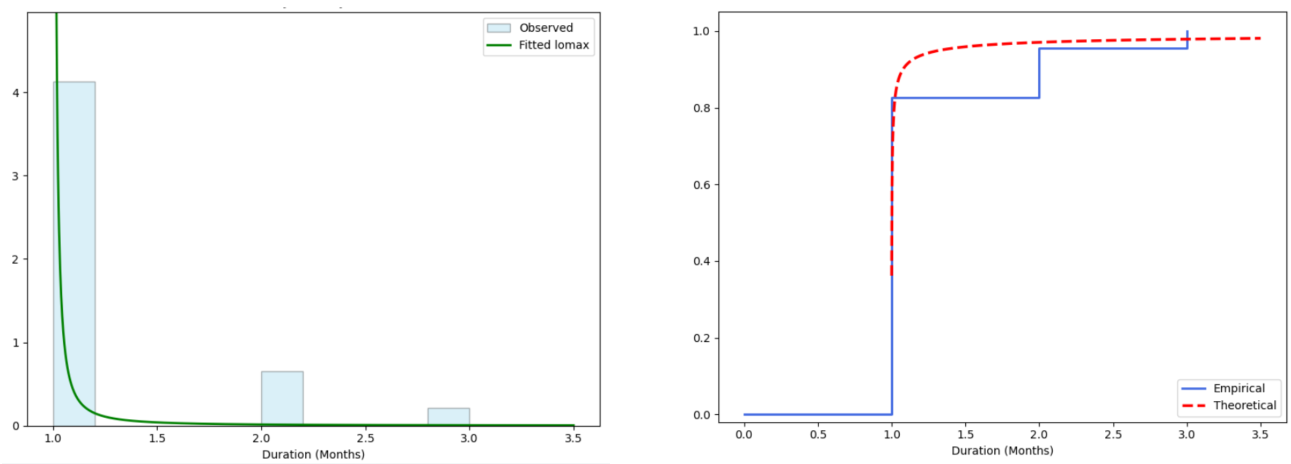

(a) Davao de Oro

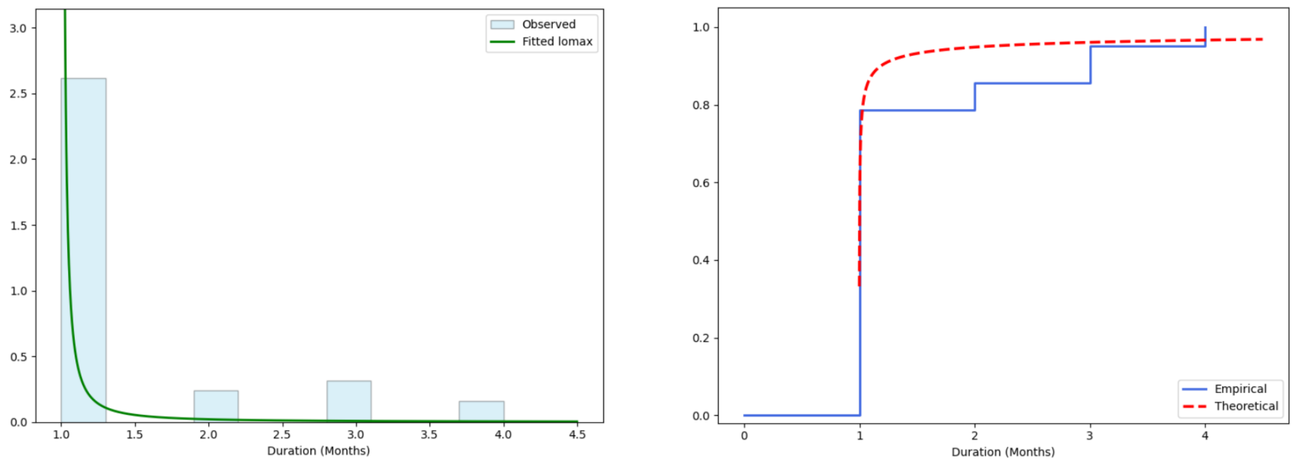

(b) Davao del Norte

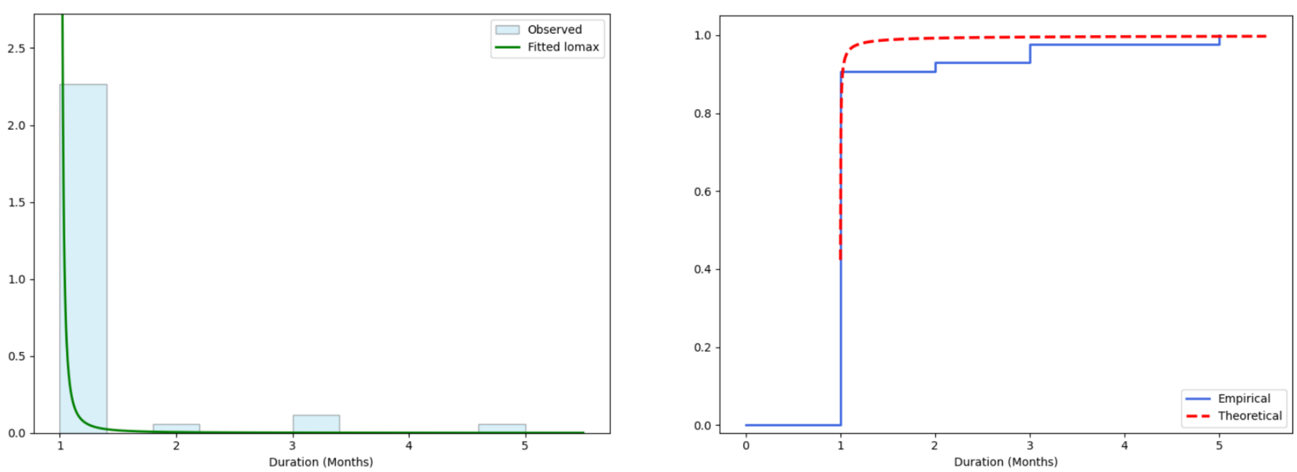

(c) Davao del Sur

FIGURE 2. Fitted Lomax PDF and cumulative distribution functions (CDFs) of flood duration across selected provinces in Region XI, Philippines.

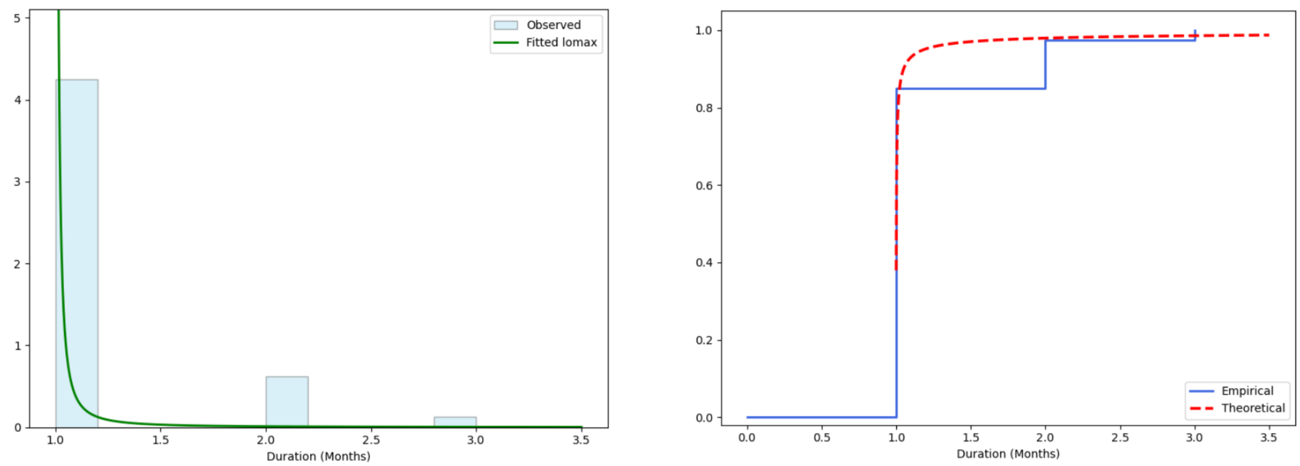

(d) Davao Occidental

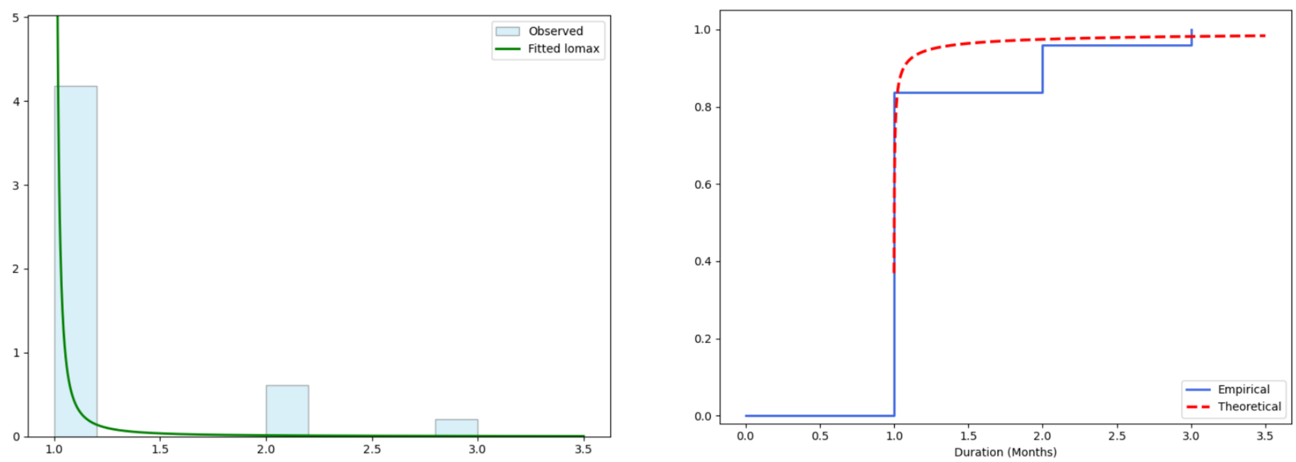

(e) Davao Oriental

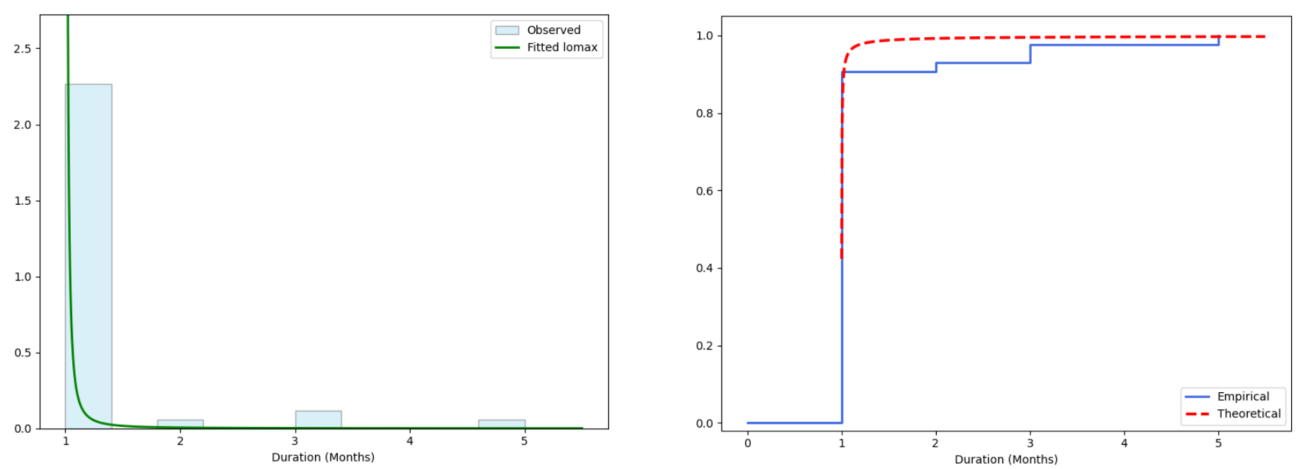

(f) Davao City

FIGURE 2. (continued).

The comparative evaluation of candidate distributions for flood peak (P) is summarized in Table 6. While the generalized gamma distribution emerged as the optimal architecture for the majority of regional stations, the selection process strictly adhered to the hierarchical protocol of statistical priority.

Specifically, a candidate model was required to satisfy the Anderson–Darling significance threshold $(p > 0.05)$ before being adjudicated based on minimum AIC and BIC values.

Under this framework, location-specific superiorities were identified; for instance, the fatigue life distribution was selected for Davao Occidental as it provided the most parsimonious fit among the statistically acceptable candidates. Conversely, the inverse Gaussian distribution was systematically rejected across all locations due to non-significance $(p < 0.05)$. Graphical diagnostics (Figure 3) confirm that these selected models effectively reconcile central tendencies with the high-intensity upper-tail extremes, providing a robust, site-specific foundation for multivariate dependence modeling.

TABLE 6. Comparative Evaluation of Probability Distributions and Parameter Estimates for Regional Flood Peak Modeling

Location	Distribution	Parameter	AD Stat	AD p-value	RMSE	AIC	BIC
Davao City	Gen Gamma	Shape(a): 0.6949, Shape(c): 1.0742, Loc: 1.0294, Scale: 0.5499	3.8350	0.0567	0.1093	30.275	37.319
	Fatigue Life	Shape(γ): 0.8951, Loc(ξ): 0.9690, Scale(β): 0.4176	0.1609	0.9500	0.0257	36.597	41.881
	Log-normal	Shape(σ): 0.8733, Loc(γ): 0.9831, Scale(e^{μ}): 0.3983	0.2007	0.8400	0.0288	37.206	42.490
	Johnson SB	Shape(γ): 2.3054, Shape(δ): 0.9422, Loc(ξ): 1.0014, Scale(λ): 4.8669	0.1656	0.9300	0.0261	38.523	45.567
	Inv Gaussian	Shape(λ): 13.5209, Loc(γ): 1.0284, Scale(μ): 0.0389	17.7431	0.0000	0.2847	115.849	121.132
Davao de Oro	Gen Gamma	Shape(a): 0.3286, Shape(c): 1.9134, Loc: 1.0006, Scale: 0.9437	2.9591	0.1600	0.0988	8.879	16.193
	Fatigue Life	Shape(γ): 0.5835, Loc(ξ): 0.8248, Scale(β): 0.5492	0.3655	0.3000	0.0334	28.856	34.342
	Log-normal	Shape(σ): 0.5336, Loc(γ): 0.7956, Scale(e^{μ}): 0.5868	0.3524	0.3033	0.0326	29.708	35.194
	Johnson SB	Shape(γ): 0.7105, Shape(δ): 0.7045, Loc(ξ): 0.9850, Scale(λ): 1.4997	0.2914	0.5733	0.0335	25.742	33.056
	Inv Gaussian	Shape(λ): 11.7177, Loc(γ): 0.9996, Scale(μ): 0.0400	19.2501	0.0000	0.2840	116.290	121.776
Davao del Norte	Gen Gamma	Shape(a): 0.6440, Shape(c): 1.3234, Loc: 1.0004, Scale: 0.6818	1.4944	0.3767	0.0571	20.007	26.957
	Johnson SB	Shape(γ): 0.5945, Shape(δ): 0.5878, Loc(ξ): 0.9932, Scale(λ): 1.4383	0.2641	0.7133	0.0312	25.003	31.954
	Fatigue Life	Shape(γ): 0.7582, Loc(ξ): 0.8920, Scale(β): 0.4550	0.6422	0.0567	0.0468	32.150	37.363
	Log-normal	Shape(σ): 0.6942, Loc(γ): 0.8757, Scale(e^{μ}): 0.4851	0.6633	0.0367	0.0490	33.767	38.980
	Inv Gaussian	Shape(λ): 13.9019, Loc(γ): 0.9994, Scale(μ): 0.0345	17.0684	0.0000	0.2777	104.543	109.756
Davao del Sur	Gen Gamma	Shape(a): 0.6949, Shape(c): 1.0742, Loc: 1.0294, Scale: 0.5499	3.8350	0.0567	0.1093	30.275	37.319
	Fatigue Life	Shape(γ): 0.8951, Loc(ξ): 0.9690, Scale(β): 0.4176	0.1609	0.9500	0.0257	36.597	41.881
	Log-normal	Shape(σ): 0.8733, Loc(γ): 0.9831, Scale(e^{μ}): 0.3983	0.2007	0.8400	0.0288	37.206	42.490
	Johnson SB	Shape(γ): 2.3054, Shape(δ): 0.9422, Loc(ξ): 1.0014, Scale(λ): 4.8669	0.1656	0.9300	0.0261	38.523	45.567
	Inv Gaussian	Shape(λ): 13.5209, Loc(γ): 1.0284, Scale(μ): 0.0389	17.7431	0.0000	0.2847	115.849	121.132
Davao Occidental	Gen Gamma	Shape(a): 0.4531, Shape(c): 1.2163, Loc: 1.0034, Scale: 0.9834	6.2848	0.0167	0.1694	33.765	40.521
	Fatigue Life	Shape(γ): 0.5768, Loc(ξ): 0.7374, Scale(β): 0.7735	0.5511	0.0800	0.0459	52.270	57.336
	Log-normal	Shape(σ): 0.5288, Loc(γ): 0.7013, Scale(e^{μ}): 0.8185	0.5072	0.0933	0.0431	52.526	57.593
	Johnson SB	Shape(γ): 2.2345, Shape(δ): 1.1639, Loc(ξ): 0.8811, Scale(λ): 4.8841	0.6047	0.0267	0.0489	54.079	60.834
	Inv Gaussian	Shape(λ): 19.9400, Loc(γ): 1.0024, Scale(μ): 0.0320	21.9376	0.0000	0.3196	137.283	142.350
Davao Oriental	Gen Gamma	Shape(a): 0.5908, Shape(c): 1.2513, Loc: 1.0021, Scale: 0.8420	0.9640	0.6833	0.0420	19.279	26.846
	Fatigue Life	Shape(γ): 0.8686, Loc(ξ): 0.9242, Scale(β): 0.4062	0.2693	0.6167	0.0284	36.577	42.252
	Log-normal	Shape(σ): 0.8278, Loc(γ): 0.9304, Scale(e^{μ}): 0.4026	0.2647	0.5867	0.0273	37.364	43.039
	Johnson SB	Shape(γ): 1.7543, Shape(δ): 0.8397, Loc(ξ): 0.9749, Scale(λ): 3.2560	0.3023	0.5167	0.0315	37.735	45.302
	Inv Gaussian	Shape(λ): 15.2427, Loc(γ): 1.0011, Scale(μ): 0.0317	20.1283	0.0000	0.2826	117.762	123.437

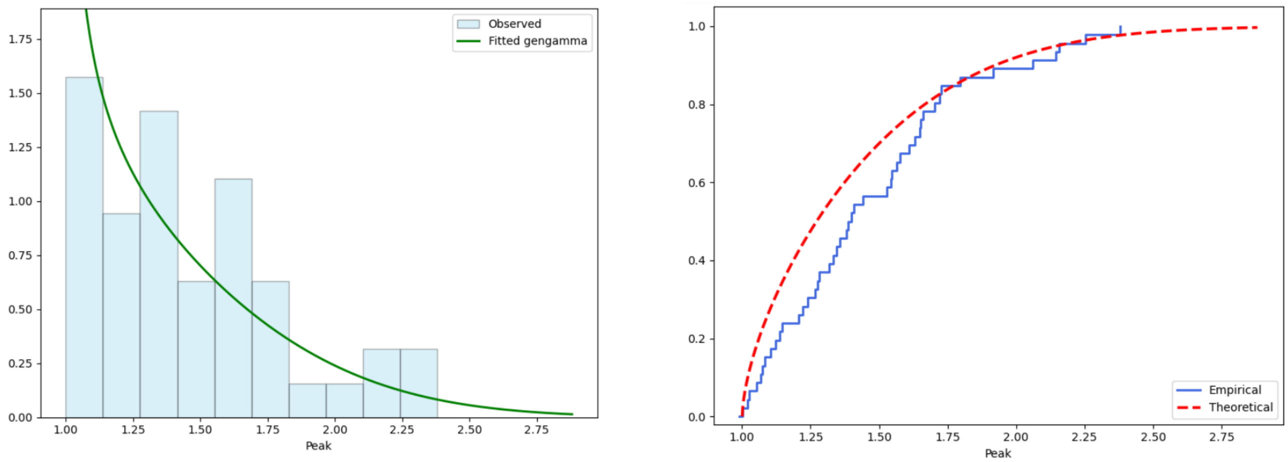

(a) Davao de Oro

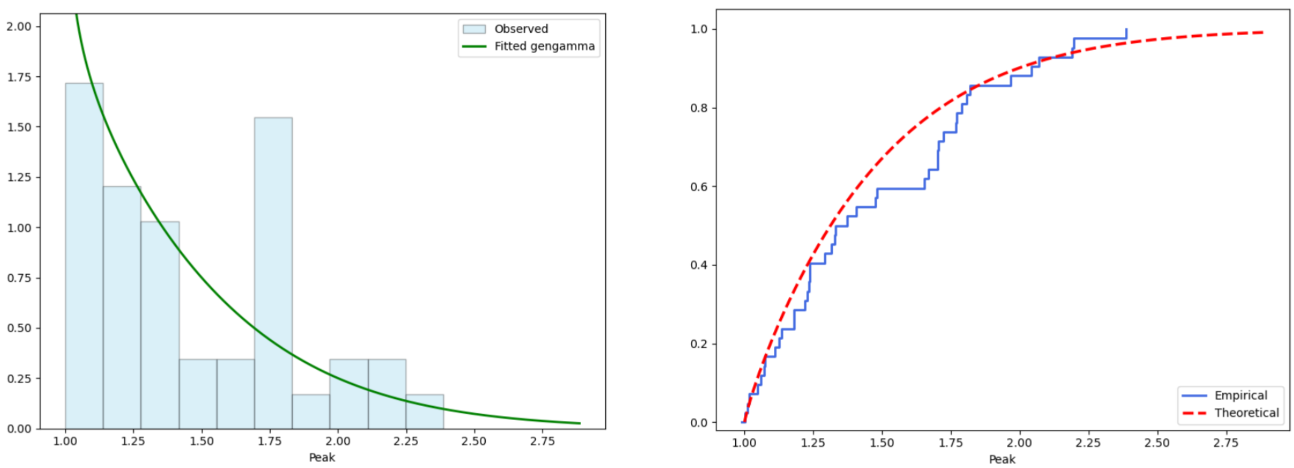

(b) Davao del Norte

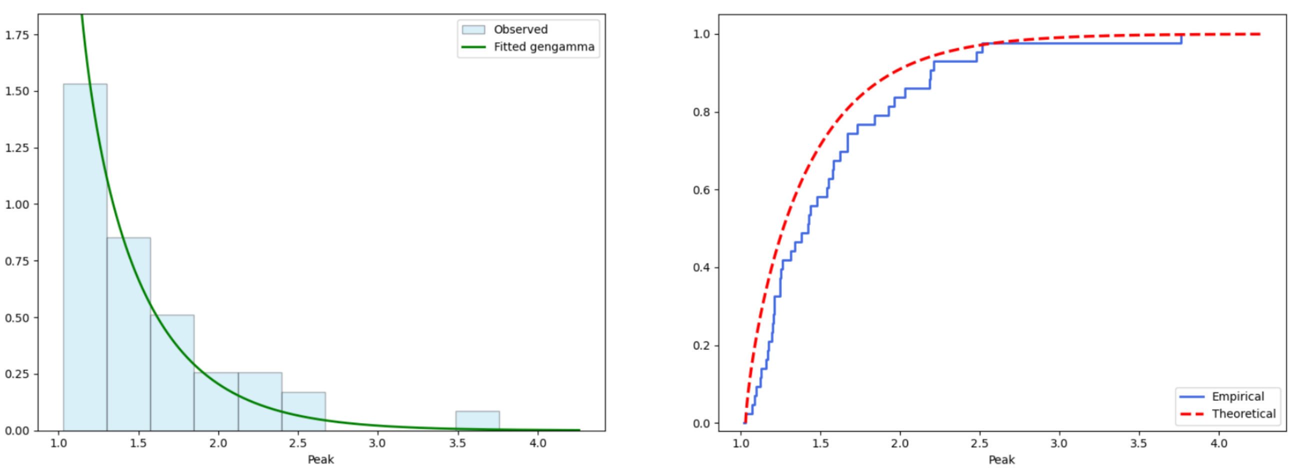

(c) Davao del Sur

FIGURE 3. Fitted probability density functions (PDFs) and cumulative distribution functions (CDFs) of flood Peak across selected provinces in Region XI, Philippines.

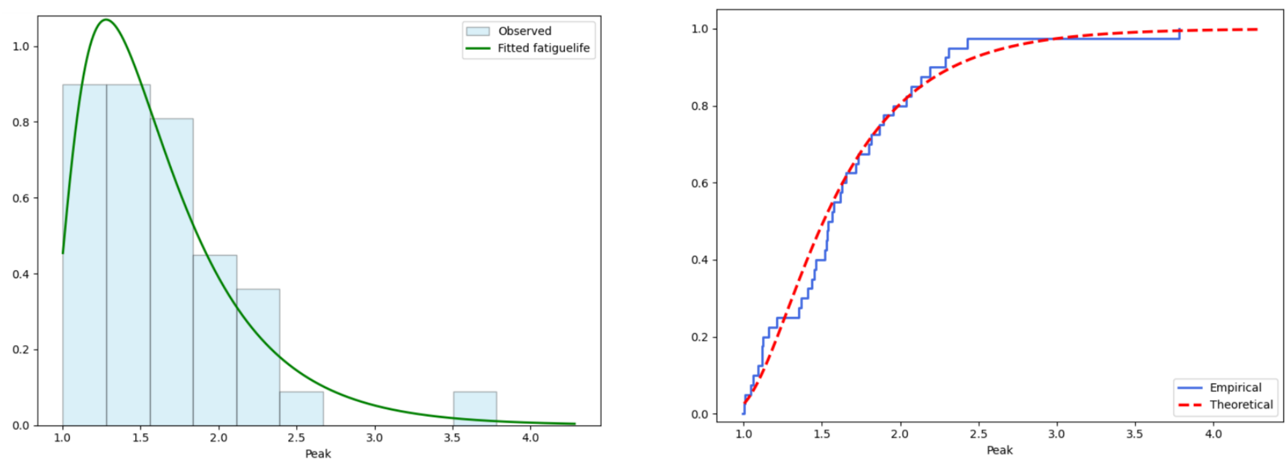

(d) Davao Occidental

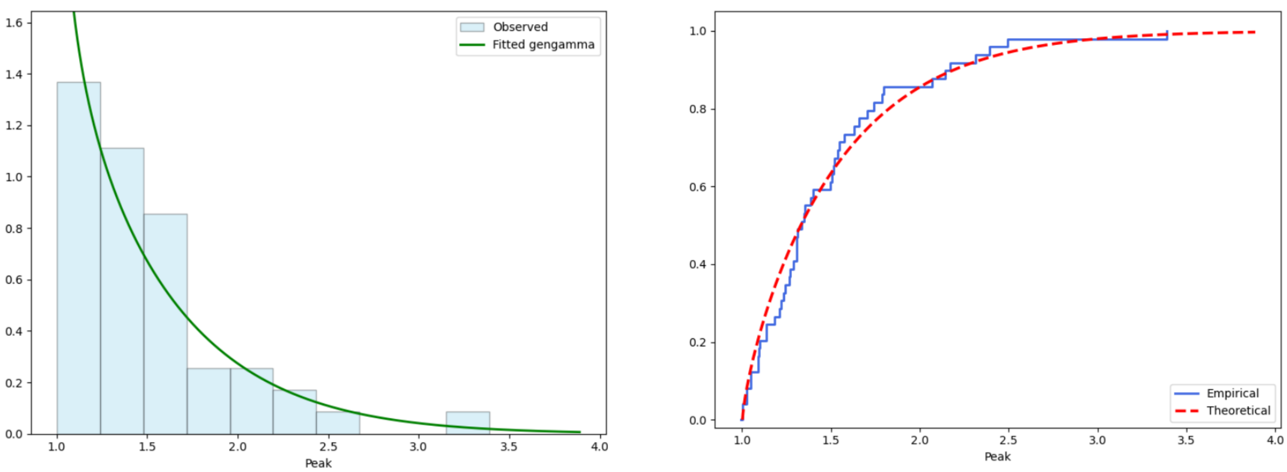

(e) Davao Oriental

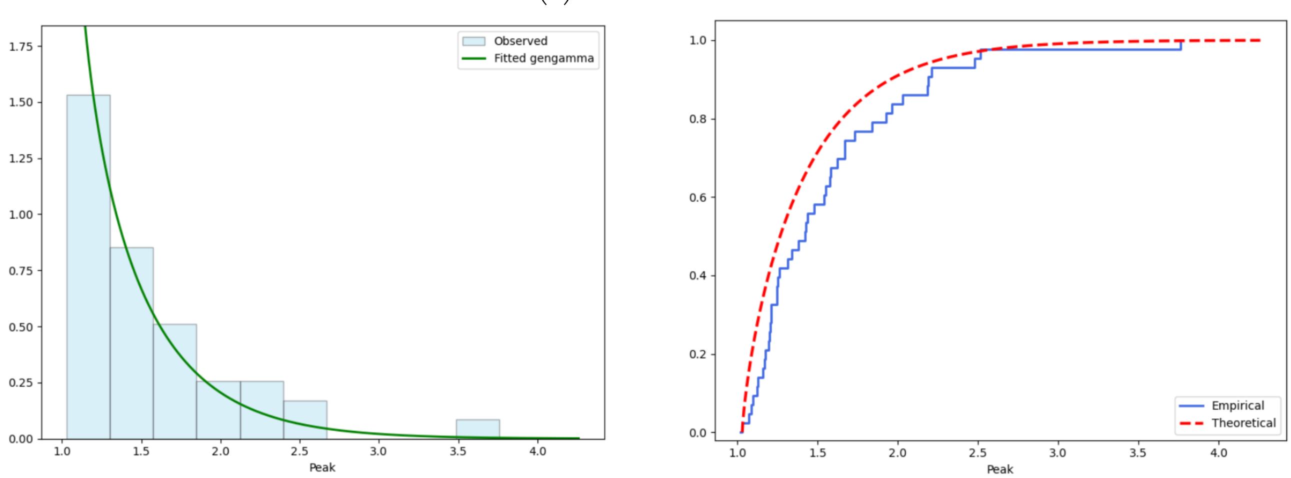

(f) Davao City

Figure 3. (continued).

The characterization of flood severity (S) necessitates the application of flexible, right-skewed distributions to capture the high-magnitude anomalies prevalent in the regional dataset. Candidate models were adjudicated using a hierarchical selection process: initial screening via the Anderson–Darling

(AD) test $(p > 0.05)$ to ensure statistical validity, followed by the minimization of AIC and BIC to optimize parsimony.

As detailed in Table 7, the beta prime and log-normal distributions emerged as the dominant architectures across the region. In the majority of locations, specifically Davao de Oro, Davao del Norte, Davao Occidental, and Davao Oriental, the beta prime distribution was selected as the optimal marginal model, consistently yielding the lowest information criteria. Conversely, for Davao City and Davao del Sur, the log-normal distribution provided a superior fit, demonstrating higher AD p-values and enhanced efficiency in modeling localized severity.

In contrast, the inverse Gaussian distribution was systematically rejected at all stations for failing the 5% significance threshold $(p < 0.05)$. Graphical diagnostics in Figure 4 corroborate these selections, illustrating that the chosen distributions effectively reconcile central tendency variability with the extreme upper-tail behavior characteristic of the region's hydrological regime. This localized selection strategy ensures a robust foundation for the subsequent multivariate dependence analysis.

TABLE 7. Comparative Evaluation of Probability Distributions and Parameter Estimates for Regional Flood Severity Modeling

Location	Distribution	Parameter	AD Stat	AD p-value	RMSE	AIC	BIC
Davao City	Log-normal	Shape(σ): 1.0315, Loc(γ): 0.0007, Scale(e^{μ}): 0.3979	0.1575	0.9500	0.0261	51.436	56.720
	Inverse Gamma	Shape(α): 1.8210, Loc(γ): -0.0768, Scale(β): 0.6914	0.1835	0.8633	0.0273	52.419	57.703
	Beta Prime	Shape(α): 1.2783, Shape(β): 3.5032, Loc(γ): 0.0253, Scale: 1.2682	0.2136	0.9567	0.0290	53.548	60.593
	Fisk	Shape(α): 1.4248, Loc(γ): 0.0284, Scale(β): 0.3585	0.2343	0.7533	0.0248	53.594	58.877
	Inverse Gaussian	Shape(λ): 16.4532, Loc(γ): 0.0284, Scale(μ): 0.0385	17.1387	0.0000	0.2801	125.408	130.692
Davao de Oro	Log-normal	Shape(σ): 0.7331, Loc(γ): -0.1050, Scale(e^{μ}): 0.4946	0.2963	0.4600	0.0306	43.212	48.698
	Inverse Gamma	Shape(α): 4.2258, Loc(γ): -0.2975, Scale(β): 2.7094	0.2869	0.4833	0.0300	44.282	49.768
	Beta Prime	Shape(α): 1.1213, Shape(β): 9.44e+10, Loc(γ): -0.0012, Scale: 4.48e+10	0.2912	0.8633	0.0295	41.954	49.269
	Fisk	Shape(α): 1.5070, Loc(γ): -0.0004, Scale(β): 0.3739	0.8142	0.0433	0.0467	48.720	54.206
	Inverse Gaussian	Shape(λ): 13.4287, Loc(γ): -0.0004, Scale(μ): 0.0397	18.9997	0.0000	0.2823	125.546	131.032
Davao del Norte	Log-normal	Shape(σ): 0.9724, Loc(γ): -0.0530, Scale(e^{μ}): 0.4250	0.2874	0.4867	0.0307	50.958	56.171
	Inverse Gamma	Shape(α): 2.4959, Loc(γ): -0.2011, Scale(β): 1.2651	0.3361	0.3433	0.0346	53.187	58.400
	Beta Prime	Shape(α): 0.8618, Shape(β): 1.4544, Loc(γ): 0.0004, Scale: 0.6485	1.4988	0.1867	0.0570	45.220	52.170
	Fisk	Shape(α): 1.2982, Loc(γ): -0.0006, Scale(β): 0.3643	0.5883	0.2633	0.0387	54.036	59.249
	Inverse Gaussian	Shape(λ): 17.2738, Loc(γ): -0.0006, Scale(μ): 0.0342	16.6790	0.0000	0.2749	117.360	122.573
Davao del Sur	Log-normal	Shape(σ): 1.0315, Loc(γ): 0.0007, Scale(e^{μ}): 0.3979	0.1575	0.9500	0.0261	51.436	56.720
	Inverse Gamma	Shape(α): 1.8210, Loc(γ): -0.0768, Scale(β): 0.6914	0.1835	0.8633	0.0273	52.419	57.703
	Beta Prime	Shape(α): 1.2783, Shape(β): 3.5032, Loc(γ): 0.0253, Scale: 1.2682	0.2136	0.9567	0.0290	53.548	60.593
	Fisk	Shape(α): 1.4248, Loc(γ): 0.0284, Scale(β): 0.3585	0.2343	0.7533	0.0248	53.594	58.877
	Inverse Gaussian	Shape(λ): 16.4532, Loc(γ): 0.0284, Scale(μ): 0.0385	17.1387	0.0000	0.2801	125.408	130.692
Davao Occidental	Log-normal	Shape(σ): 0.6889, Loc(γ): -0.1834, Scale(e^{μ}): 0.7144	0.4523	0.1433	0.0428	62.795	67.862
	Inverse Gamma	Shape(α): 4.8179, Loc(γ): -0.4738, Scale(β): 4.5636	0.4121	0.1567	0.0399	63.630	68.697
	Beta Prime	Shape(α): 0.7085, Shape(β): 5.8868, Loc(γ): 0.0034, Scale: 5.3572	2.2544	0.1400	0.0877	44.184	50.939
	Fisk	Shape(α): 1.3697, Loc(γ): 0.0024, Scale(β): 0.4925	1.2916	0.0333	0.0674	69.142	74.209
	Inverse Gaussian	Shape(λ): 22.2337, Loc(γ): 0.0024, Scale(μ): 0.0319	21.7225	0.0000	0.3182	143.973	149.040
Davao Oriental	Log-normal	Shape(σ): 0.9313, Loc(γ): -0.0546, Scale(e^{μ}): 0.4066	0.2577	0.6067	0.0260	49.900	55.575
	Inverse Gamma	Shape(α): 2.6243, Loc(γ): -0.1893, Scale(β): 1.2581	0.2575	0.6433	0.0252	51.740	57.415
	Beta Prime	Shape(α): 0.9190, Shape(β): 6.7946, Loc(γ): 0.0021, Scale: 3.1664	1.2969	0.3767	0.0509	42.158	49.726
	Fisk	Shape(α): 1.3241, Loc(γ): 0.0011, Scale(β): 0.3402	0.7519	0.1167	0.0406	53.766	59.441
	Inverse Gaussian	Shape(λ): 17.3636, Loc(γ): 0.0011, Scale(μ): 0.0316	20.2247	0.0000	0.2825	128.486	134.161

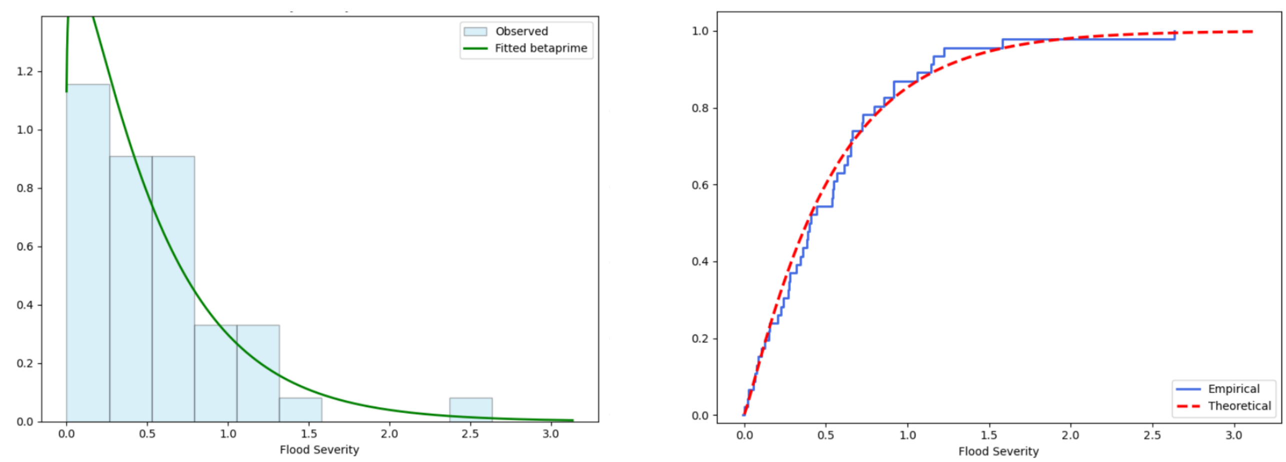

(a) Davao de Oro

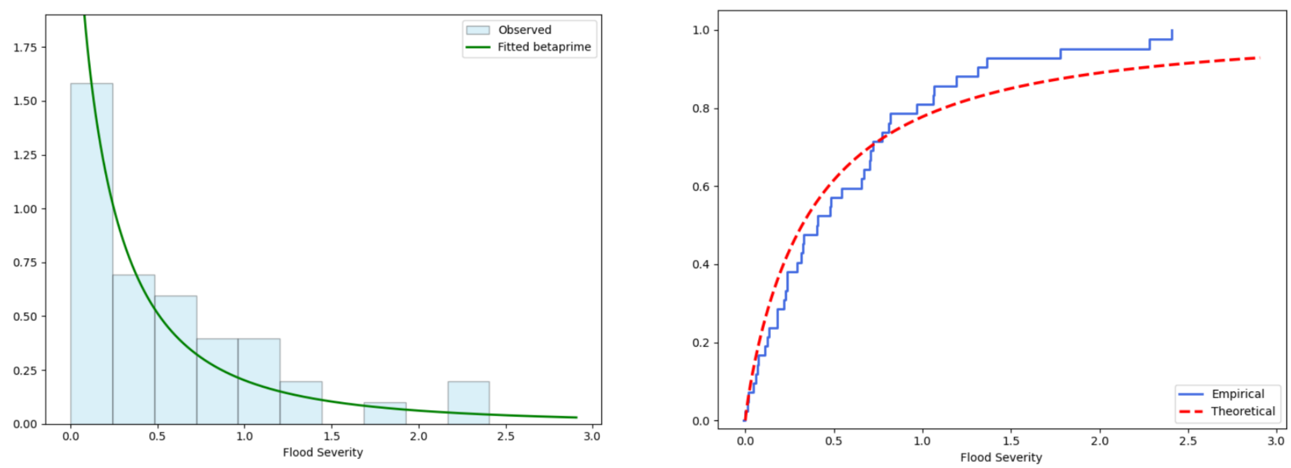

(b) Davao del Norte

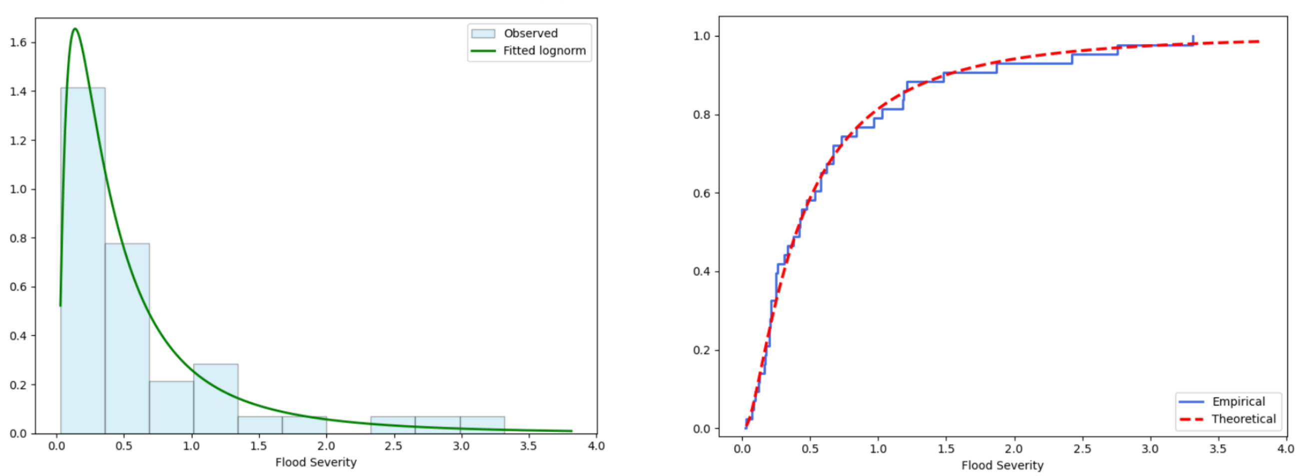

(c) Davao del Sur

FIGURE 4. Fitted probability density functions (PDFs) and cumulative distribution functions (CDFs) of flood Severity across selected provinces in Region XI, Philippines.

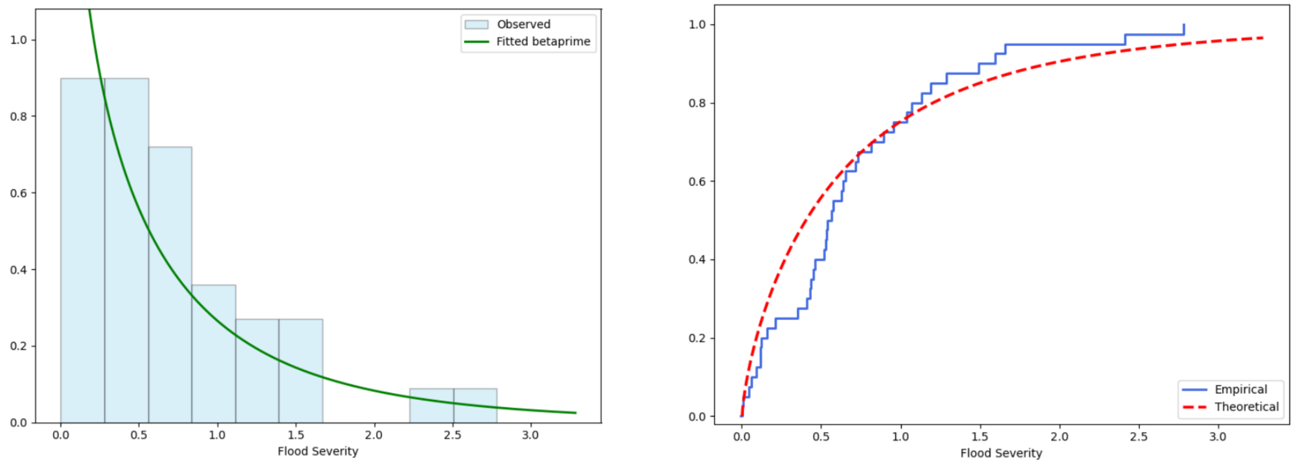

(d) Davao Occidental

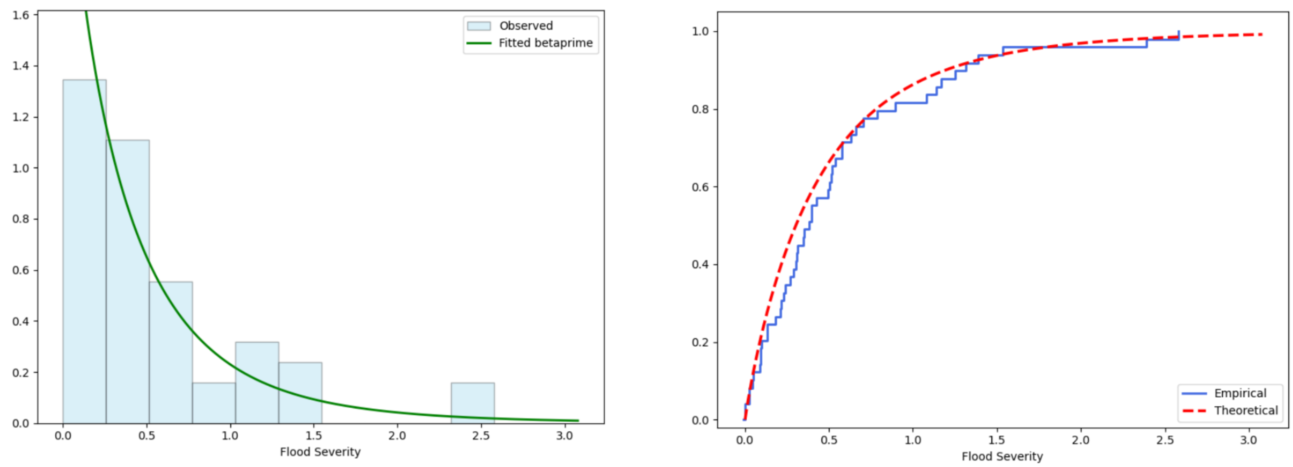

(e) Davao Oriental

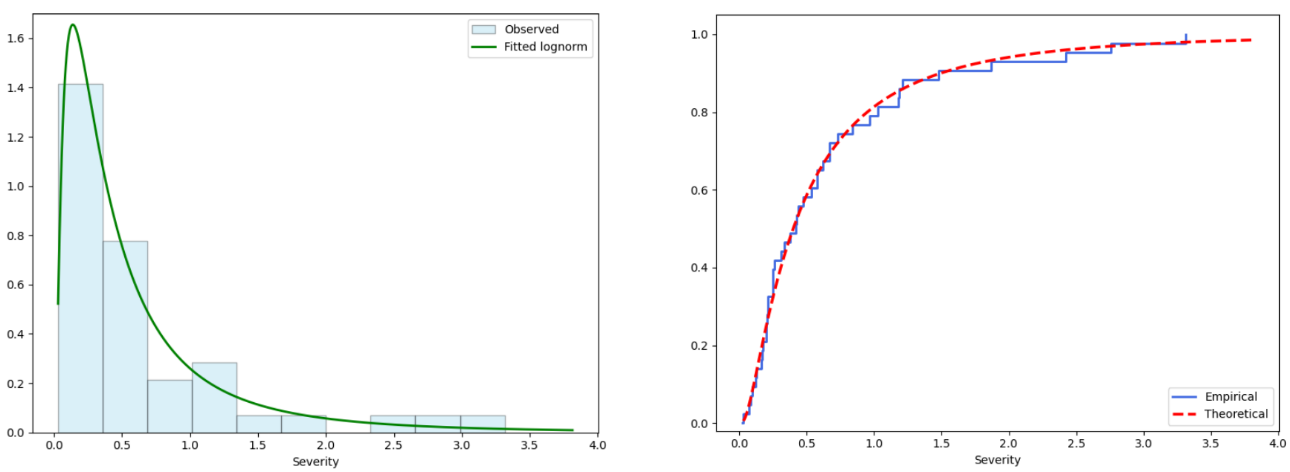

(f) Davao City

Figure 4. (continued).

3.2. **Selection of Copula Model.** This subsection identifies the most appropriate copula functions for modeling the dependence structure among flood variables. Candidate models—including Student-t, BB1, BB7, and the generalized RLUF copula with RLUF-type structure—were evaluated using RMSE, AIC, and BIC to ensure an optimal balance between goodness-of-fit and parsimony. The selected models were subsequently employed for bivariate return period estimation.

For Davao City (Table 8), the extended RLUF-type (BB7) copula provides the best fit for the duration–severity pair, yielding the lowest RMSE (0.181) and most favorable AIC (-715.36) and BIC (-699.51). For the duration–peak pair, the extended RLUF-type (BB1) copula is preferred, achieving the lowest AIC and BIC despite comparable RMSE values among competing models. These results highlight the superior flexibility of extended RLUF-type formulations in capturing tail dependence and asymmetric structures.

Table 8. Estimated Parameters and Performance Metrics of Copula Functions for Flood Characteristic Bivariate Distributions in Davao City

Pair	Model	Estimated Parameters	RMSE	AIC	BIC	LogLik
Dur-Sev	Ext. RLUF-type (BB7)	$\theta = 11.429, \delta = 0.020, a = 0.580, b = 1.858, c_1 = 0.742, c_2 = 0.786, m = 0.747, n = 2.009, \theta_2 = 2.480$	0.181	-715.36	-699.51	366.68
Dur-Sev	BB7	$\theta = 8.559, \delta = 0.0001$	0.184	-498.11	-494.58	251.05
Dur-Sev	Ext. RLUF-type (Clayton)	$\theta = 0.760, a = 0.050, b = 1.098, c_1 = 6.329, c_2 = 0.545, m = 2.439, n = 1.053, \theta_2 = -501901.91$	0.568	-70.51	-56.42	43.25
Dur-Sev	Ext. RLUF-type (Stud-t)	$\rho = 0.560, \nu = 99.54, a = 0.050, b = 1.208, c_1 = 6.480, c_2 = 0.628, m = 2.469, n = 0.983, \theta_2 = -447587.93$	0.568	-68.58	-52.73	43.29
Dur-Sev	Ext. RLUF-type (Gumbel)	$\theta = 1.560, a = 0.077, b = 0.055, c_1 = 4.449, c_2 = 8.074, m = 1.942, n = 5.000, \theta_2 = 8667.81$	0.568	-45.87	-31.78	30.93
Dur-Sev	Gumbel	$\theta = 1.704$	0.218	-11.47	-9.71	6.74
Dur-Sev	BB1	$\theta = 0.0001, \delta = 1.704$	0.218	-9.47	-5.95	6.74
Dur-Sev	Student-t	$\rho = 0.630, \nu = 100.00$	0.215	-7.08	-3.56	5.54
Dur-Sev	Ext. RLUF-type (BB1)	$\theta = 0.409, \delta = 1.451, a = 0.050, b = 3.132, c_1 = 2.972, c_2 = 0.761, m = 1.655, n = 0.929, \theta_2 = -74.62$	0.223	-1.29	14.56	9.65
Dur-Sev	Clayton	$\theta = 0.705$	0.241	-0.87	0.89	1.44
Dur-Peak	Ext. RLUF-type (BB1)	$\theta = 0.496, \delta = 1.090, a = 0.050, b = 1.976, c_1 = 6.701, c_2 = 1.060, m = 2.511, n = 1.040, \theta_2 = -1729759.08$	0.571	-72.21	-56.36	45.10
Dur-Peak	Ext. RLUF-type (Clayton)	$\theta = 0.426, a = 0.050, b = 1.233, c_1 = 6.831, c_2 = 0.538, m = 2.535, n = 0.972, \theta_2 = -457677.61$	0.571	-67.14	-53.05	41.57
Dur-Peak	Ext. RLUF-type (Stud-t)	$\rho = 0.493, \nu = 100.00, a = 0.058, b = 0.946, c_1 = 5.500, c_2 = 0.786, m = 2.246, n = 1.051, \theta_2 = -106324.41$	0.571	-50.18	-34.33	34.09
Dur-Peak	Ext. RLUF-type (Gumbel)	$\theta = 1.444, a = 0.050, b = 1.223, c_1 = 5.218, c_2 = 1.047, m = 2.201, n = 1.015, \theta_2 = -92657.95$	0.571	-49.40	-35.31	32.70
Dur-Peak	Ext. RLUF-type (BB7)	$\theta = 1.616, \delta = 2.253, a = 0.050, b = 1.300, c_1 = 3.876, c_2 = 1.013, m = 1.852, n = 1.023, \theta_2 = -4432.88$	0.571	-11.72	4.13	14.86
Dur-Peak	Gumbel	$\theta = 1.328$	0.236	-1.56	0.20	1.78
Dur-Peak	Student-t	$\rho = 0.498, \nu = 100.00$	0.225	-0.77	2.75	2.39
Dur-Peak	Clayton	$\theta = 0.592$	0.241	-0.06	1.70	1.03
Dur-Peak	BB1	$\theta = 0.201, \delta = 1.269$	0.232	0.18	3.70	1.91
Dur-Peak	BB7	$\theta = 1.330, \delta = 0.356$	0.235	0.46	3.98	1.77

For Davao de Oro (Table 9), the extended RLUF-type (BB1) copula best represents the duration–severity relationship, while the extended RLUF-type (Student-t) copula is optimal for duration–peak. Both selections are supported by the lowest AIC and BIC values, indicating superior efficiency. The presence of negative dependence in the Student-t model suggests localized hydrological dynamics, such as short-duration high-intensity events.

Table 9. Estimated Parameters and Performance Metrics of Copula Functions for Flood Characteristic Bivariate Distributions in Davao de Oro

Pair	Model	Estimated Parameters	RMSE	AIC	BIC	LogLik
Dur-Sev	Ext. RLUF-type (BB1)	$\theta = 3.553, \delta = 1.000, a = 0.266, b = 0.050, c_1 = 9.009, c_2 = 5.755, m = 5.000, n = 5.000, \theta_2 = 1.498 \times 10^7$	0.584	-237.48	-221.02	127.74
Dur-Sev	Ext. RLUF-type (Clayton)	$\theta = 9.020, a = 0.050, b = 1.456, c_1 = 10.000, c_2 = 2.697, m = 2.058, n = 0.849, \theta_2 = -8.273 \times 10^7$	0.584	-136.80	-122.17	76.40
Dur-Sev	Ext. RLUF-type (Gumbel)	$\theta = 2.288, a = 0.050, b = 0.235, c_1 = 8.378, c_2 = 0.440, m = 2.320, n = 1.033, \theta_2 = -3.389 \times 10^7$	0.584	-133.99	-119.36	75.00
Dur-Sev	Ext. RLUF-type (Stud-t)	$\rho = -0.695, \nu = 99.971, a = 0.051, b = 0.460, c_1 = 9.045, c_2 = 1.174, m = 2.408, n = 0.549, \theta_2 = -3.181 \times 10^6$	0.584	-132.73	-116.27	75.36
Dur-Sev	Ext. RLUF-type (BB7)	$\theta = 1.714, \delta = 0.256, a = 0.050, b = 0.564, c_1 = 7.543, c_2 = 1.201, m = 2.196, n = 0.797, \theta_2 = -1.920 \times 10^6$	0.584	-123.20	-106.74	70.60
Dur-Sev	Gumbel	$\theta = 1.492$	0.200	-7.51	-5.68	4.75
Dur-Sev	Student-t	$\rho = 0.577, \nu = 100.00$	0.192	-5.92	-2.26	4.96
Dur-Sev	BB7	$\theta = 1.606, \delta = 0.279$	0.203	-5.54	-1.88	4.77
Dur-Sev	BB1	$\theta = 0.048, \delta = 1.474$	0.199	-5.53	-1.87	4.76
Dur-Sev	Clayton	$\theta = 0.737$	0.209	-1.90	-0.07	1.95
Dur-Peak	Ext. RLUF-type (Stud-t)	$\rho = -0.374, \nu = 99.933, a = 0.205, b = 0.323, c_1 = 9.989, c_2 = 0.921, m = 2.283, n = 0.496, \theta_2 = -9.591 \times 10^6$	0.592	-140.94	-124.48	79.47
Dur-Peak	Ext. RLUF-type (BB7)	$\theta = 1.040, \delta = 0.007, a = 0.050, b = 0.235, c_1 = 9.052, c_2 = 0.663, m = 2.411, n = 0.502, \theta_2 = -5.532 \times 10^6$	0.592	-139.43	-122.97	78.72
Dur-Peak	Ext. RLUF-type (BB1)	$\theta = 0.0001, \delta = 1.576, a = 0.050, b = 0.563, c_1 = 9.672, c_2 = 1.757, m = 2.489, n = 0.439, \theta_2 = -6.736 \times 10^6$	0.592	-132.73	-116.27	75.36
Dur-Peak	Ext. RLUF-type (Gumbel)	$\theta = 1.448, a = 0.067, b = 0.242, c_1 = 8.377, c_2 = 0.543, m = 2.290, n = 0.761, \theta_2 = -2.126 \times 10^6$	0.592	-126.63	-112.00	71.31
Dur-Peak	Ext. RLUF-type (Clayton)	$\theta = 0.0001, a = 0.050, b = 0.414, c_1 = 8.056, c_2 = 1.001, m = 2.274, n = 0.668, \theta_2 = -2.505 \times 10^6$	0.592	-124.64	-110.01	70.32
Dur-Peak	Gumbel	$\theta = 1.235$	0.212	-0.66	1.17	1.33
Dur-Peak	Clayton	$\theta = 0.562$	0.209	-0.30	1.53	1.15
Dur-Peak	Student-t	$\rho = 0.434, \nu = 100.00$	0.199	-0.10	3.55	2.05
Dur-Peak	BB1	$\theta = 0.282, \delta = 1.164$	0.205	0.87	4.53	1.56
Dur-Peak	BB7	$\theta = 1.209, \delta = 0.398$	0.207	0.98	4.64	1.51

For Davao del Norte (Table 10), the extended RLUF-type (BB7) copula is selected for duration–severity, while the extended RLUF-type (Clayton) copula is preferred for duration–peak. Both models achieve the lowest information criteria, confirming improved fit relative to classical copulas.

TABLE 10. Estimated Parameters and Performance Metrics of Copula Functions for Flood Characteristic Bivariate Distributions in Davao del Norte

Pair	Model	Estimated Parameters	RMSE	AIC	BIC	LogLik
Dur-Sev	Ext. RLUF-type (BB7)	$\theta = 1.013, \delta = 0.018, a = 0.080, b = 2.511, c_1 = 10.0, c_2 = 0.052, m = 5.0, n = 0.538, \theta_2 = -4.459 \times 10^7$	0.576	-402.54	-386.90	210.27
Dur-Sev	Ext. RLUF-type (Clayton)	$\theta = 0.005, a = 0.651, b = 0.101, c_1 = 10.0, c_2 = 5.940, m = 5.0, n = 5.0, \theta_2 = 6.049 \times 10^6$	0.576	-277.13	-263.23	146.57
Dur-Sev	Ext. RLUF-type (Stud-t)	$\rho = -0.950, \nu = 100.0, a = 0.062, b = 1.302, c_1 = 9.329, c_2 = 0.451, m = 3.083, n = 0.824, \theta_2 = -4.535 \times 10^7$	0.576	-271.90	-256.27	144.95
Dur-Sev	Ext. RLUF-type (Gumbel)	$\theta = 1.719, a = 0.050, b = 3.343, c_1 = 8.940, c_2 = 3.259, m = 2.186, n = 1.026, \theta_2 = -8.544 \times 10^6$	0.576	-177.26	-163.35	96.63
Dur-Sev	Ext. RLUF-type (BB1)	$\theta = 3.651, \delta = 1.000, a = 0.050, b = 2.081, c_1 = 7.664, c_2 = 2.102, m = 2.011, n = 1.029, \theta_2 = -8.596 \times 10^5$	0.576	-137.30	-121.66	77.65
Dur-Sev	Gumbel	$\theta = 1.780$	0.182	-15.06	-13.32	8.53
Dur-Sev	Student-t	$\rho = 0.695, \nu = 100.0$	0.175	-13.79	-10.32	8.90
Dur-Sev	BB1	$\theta = 0.0001, \delta = 1.780$	0.182	-13.06	-9.58	8.53
Dur-Sev	BB7	$\theta = 1.994, \delta = 0.309$	0.187	-12.61	-9.14	8.31
Dur-Sev	Clayton	$\theta = 1.077$	0.192	-5.76	-4.02	3.88
Dur-Peak	Ext. RLUF-type (Clayton)	$\theta = 1.895, a = 0.050, b = 0.872, c_1 = 8.426, c_2 = 0.964, m = 2.119, n = 0.991, \theta_2 = -4.655 \times 10^6$	0.583	-189.49	-175.59	102.75
Dur-Peak	Ext. RLUF-type (Student-t)	$\rho = -0.105, \nu = 100.0, a = 0.050, b = 0.774, c_1 = 8.356, c_2 = 0.527, m = 2.109, n = 1.572, \theta_2 = -4.044 \times 10^6$	0.583	-186.53	-170.89	102.26
Dur-Peak	Ext. RLUF-type (BB1)	$\theta = 0.360, \delta = 1.324, a = 0.050, b = 0.881, c_1 = 7.567, c_2 = 1.057, m = 1.997, n = 0.962, \theta_2 = -1.258 \times 10^6$	0.583	-165.24	-149.60	91.62
Dur-Peak	Ext. RLUF-type (BB7)	$\theta = 1.015, \delta = 3.750, a = 0.050, b = 0.739, c_1 = 7.254, c_2 = 1.187, m = 1.949, n = 0.864, \theta_2 = -7.397 \times 10^5$	0.583	-131.07	-115.43	74.53
Dur-Peak	Ext. RLUF-type (Gumbel)	$\theta = 1.318, a = 0.050, b = 0.768, c_1 = 5.504, c_2 = 0.775, m = 1.638, n = 1.059, \theta_2 = -1.789 \times 10^4$	0.583	-93.61	-79.71	54.80
Dur-Peak	Gumbel	$\theta = 1.514$	0.189	-7.06	-5.33	4.53
Dur-Peak	Student-t	$\rho = 0.599, \nu = 100.0$	0.179	-6.69	-3.21	5.34
Dur-Peak	BB1	$\theta = 0.179, \delta = 1.443$	0.186	-5.27	-1.79	4.63
Dur-Peak	BB7	$\theta = 1.569, \delta = 0.433$	0.190	-4.79	-1.31	4.39
Dur-Peak	Clayton	$\theta = 0.895$	0.192	-3.61	-1.87	2.81

For Davao del Sur (Table 11), the extended RLUF-type (BB7) copula provides the best fit for duration–severity, while the extended RLUF-type (BB1) copula is optimal for duration–peak. The results further confirm strong upper-tail dependence, indicating that prolonged events are associated with increased severity.

TABLE 11. Estimated Parameters and Performance Metrics of Copula Functions for Flood Characteristic Bivariate Distributions in Davao del Sur

Pair	Model	Estimated Parameters	RMSE	AIC	BIC	LogLik
Dur-Sev	Ext. RLUF-type (BB7)	$\theta = 11.429, \delta = 0.020, a = 0.580, b = 1.858, c_1 = 0.742, c_2 = 0.786, m = 0.747, n = 2.009, \theta_2 = 2.480$	0.181	-715.36	-699.51	366.68
Dur-Sev	BB7	$\theta = 8.559, \delta = 0.0001$	0.184	-498.11	-494.58	251.05
Dur-Sev	Ext. RLUF-type (Clayton)	$\theta = 0.760, a = 0.050, b = 1.098, c_1 = 6.329, c_2 = 0.545, m = 2.439, n = 1.053, \theta_2 = -5.019 \times 10^5$	0.568	-70.51	-56.42	43.25
Dur-Sev	Ext. RLUF-type (Stud-t)	$\rho = 0.560, \nu = 99.541, a = 0.050, b = 1.208, c_1 = 6.480, c_2 = 0.628, m = 2.469, n = 0.983, \theta_2 = -4.476 \times 10^5$	0.568	-68.58	-52.73	43.29
Dur-Sev	Ext. RLUF-type (Gumbel)	$\theta = 1.560, a = 0.077, b = 0.055, c_1 = 4.449, c_2 = 8.074, m = 1.942, n = 5.0, \theta_2 = 8667.81$	0.568	-45.87	-31.78	30.93
Dur-Sev	Gumbel	$\theta = 1.704$	0.218	-11.47	-9.71	6.74
Dur-Sev	BB1	$\theta = 0.0001, \delta = 1.704$	0.218	-9.47	-5.95	6.74
Dur-Sev	Student-t	$\rho = 0.630, \nu = 100.0$	0.215	-7.08	-3.56	5.54
Dur-Sev	Ext. RLUF-type (BB1)	$\theta = 0.409, \delta = 1.451, a = 0.050, b = 3.132, c_1 = 2.972, c_2 = 0.761, m = 1.655, n = 0.929, \theta_2 = -74.62$	0.223	-1.29	14.56	9.65
Dur-Sev	Clayton	$\theta = 0.705$	0.241	-0.87	0.89	1.44
Dur-Peak	Ext. RLUF-type (BB1)	$\theta = 0.496, \delta = 1.090, a = 0.050, b = 1.976, c_1 = 6.701, c_2 = 1.060, m = 2.511, n = 1.040, \theta_2 = -1.730 \times 10^6$	0.571	-72.21	-56.36	45.10
Dur-Peak	Ext. RLUF-type (Clayton)	$\theta = 0.426, a = 0.050, b = 1.233, c_1 = 6.831, c_2 = 0.538, m = 2.535, n = 0.972, \theta_2 = -4.577 \times 10^5$	0.571	-67.14	-53.05	41.57
Dur-Peak	Ext. RLUF-type (Stud-t)	$\rho = 0.493, \nu = 99.997, a = 0.058, b = 0.946, c_1 = 5.500, c_2 = 0.786, m = 2.246, n = 1.051, \theta_2 = -1.063 \times 10^5$	0.571	-50.18	-34.33	34.09
Dur-Peak	Ext. RLUF-type (Gumbel)	$\theta = 1.444, a = 0.050, b = 1.223, c_1 = 5.218, c_2 = 1.047, m = 2.201, n = 1.015, \theta_2 = -9.266 \times 10^4$	0.571	-49.40	-35.31	32.70
Dur-Peak	Ext. RLUF-type (BB7)	$\theta = 1.616, \delta = 2.253, a = 0.050, b = 1.300, c_1 = 3.876, c_2 = 1.013, m = 1.852, n = 1.023, \theta_2 = -4432.88$	0.571	-11.72	4.13	14.86
Dur-Peak	Gumbel	$\theta = 1.328$	0.236	-1.56	0.20	1.78
Dur-Peak	Student-t	$\rho = 0.498, \nu = 100.0$	0.225	-0.77	2.75	2.39
Dur-Peak	Clayton	$\theta = 0.592$	0.241	-0.06	1.70	1.03
Dur-Peak	BB1	$\theta = 0.201, \delta = 1.269$	0.232	0.18	3.70	1.91
Dur-Peak	BB7	$\theta = 1.330, \delta = 0.356$	0.235	0.46	3.98	1.77

For Davao Occidental (Table 12), the extended RLUF-type (Student-t) copula best captures the duration–severity dependence, whereas the extended RLUF-type (BB1) copula is selected for duration–peak.

Despite lower RMSE in some alternatives, information criteria indicate overfitting, reinforcing the robustness of the selected models.

TABLE 12. Estimated Parameters and Performance Metrics of Copula Functions for Flood Characteristic Bivariate Distributions in Davao Occidental

Pair	Model	Estimated Parameters	RMSE	AIC	BIC	LogLik
Dur–Sev	Ext. RLUF-type (Stud-t)	$\rho = -0.076, \nu = 99.999, a = 0.050, b = 0.421, c_1 = 8.302, c_2 = 0.804, m = 2.444, n = 0.536, \theta_2 = -2.145\times 10^6$	0.580	-99.86	-84.66	58.93
Dur–Sev	Ext. RLUF-type (Clayton)	$\theta = 0.836, a = 0.210, b = 0.787, c_1 = 7.434, c_2 = 1.276, m = 2.029, n = 0.895, \theta_2 = -1.704 \times 10^6$	0.580	-96.09	-82.58	56.05
Dur–Sev	Ext. RLUF-type (BB7)	$\theta = 1.561, \delta = 4.767, a = 0.050, b = 0.628, c_1 = 6.868, c_2 = 1.221, m = 2.217, n = 0.868, \theta_2 = -1.102\times 10^6$	0.580	-71.70	-56.50	44.85
Dur–Sev	Gumbel	$\theta = 1.521$	0.207	-6.20	-4.51	4.10
Dur–Sev	BB7	$\theta = 1.660, \delta = 0.276$	0.210	-4.40	-1.02	4.20
Dur–Sev	BB1	$\theta = 0.024, \delta = 1.511$	0.207	-4.20	-0.83	4.10
Dur–Sev	Student-t	$\rho = 0.566, \nu = 100.0$	0.202	-3.66	-0.28	3.83
Dur–Sev	Clayton	$\theta = 0.719$	0.219	-1.08	0.61	1.54
Dur–Sev	Ext. RLUF-type (BB1)	$\theta = 0.153, \delta = 1.460, a = 0.050, b = 0.967, c_1 = 1.928, c_2 = 1.350, m = 1.326, n = 0.935, \theta_2 = -80.226$	0.157	7.42	22.62	5.29
Dur–Sev	Ext. RLUF-type (Gumbel)	$\theta = 1.474, a = 0.408, b = 0.745, c_1 = 0.333, c_2 = 0.968, m = 0.100, n = 0.971, \theta_2 = 4.674$	0.205	7.59	21.11	4.20
Dur–Peak	Ext. RLUF-type (BB1)	$\theta = 0.015, \delta = 1.551, a = 0.050, b = 0.542, c_1 = 9.737, c_2 = 1.040, m = 2.462, n = 0.848, \theta_2 = -6.080\times 10^7$	0.584	-203.25	-188.05	110.63
Dur–Peak	Ext. RLUF-type (Stud-t)	$\rho = 0.438, \nu = 100.0, a = 0.050, b = 1.359, c_1 = 7.803, c_2 = 2.407, m = 2.369, n = 0.938, \theta_2 = -1.811\times 10^7$	0.584	-112.77	-97.57	65.38
Dur–Peak	Ext. RLUF-type (BB7)	$\theta = 1.452, \delta = 1.130, a = 0.050, b = 0.447, c_1 = 7.295, c_2 = 0.666, m = 2.289, n = 1.181, \theta_2 = -1.763\times 10^6$	0.584	-101.47	-86.27	59.73
Dur–Peak	Ext. RLUF-type (Gumbel)	$\theta = 1.845, a = 0.053, b = 0.407, c_1 = 7.434, c_2 = 0.842, m = 2.306, n = 0.640, \theta_2 = -9.945 \times 10^5$	0.584	-89.25	-75.74	52.63
Dur–Peak	Ext. RLUF-type (Clayton)	$\theta = 1.099, a = 0.054, b = 1.132, c_1 = 6.386, c_2 = 2.114, m = 2.122, n = 0.897, \theta_2 = -1.019 \times 10^6$	0.584	-84.65	-71.14	50.33
Dur–Peak	Gumbel	$\theta = 1.289$	0.218	-0.96	0.73	1.48
Dur–Peak	Clayton	$\theta = 0.600$	0.218	-0.17	1.51	1.09
Dur–Peak	Student-t	$\rho = 0.458, \nu = 100.0$	0.207	0.19	3.56	1.91
Dur–Peak	BB1	$\theta = 0.249, \delta = 1.218$	0.213	0.70	4.08	1.65
Dur–Peak	BB7	$\theta = 1.287, \delta = 0.392$	0.215	0.79	4.17	1.61

For Davao Oriental (Table 13), the extended RLUF-type (BB7) copula is optimal for duration–severity, while the extended RLUF-type (Clayton) copula best represents duration–peak. These models consistently outperform classical copulas, reflecting complex and asymmetric dependence structures.

Table 13. Estimated Parameters and Performance Metrics of Copula Functions for Flood Characteristic Bivariate Distributions in Davao Oriental

Pair	Model	Estimated Parameters	RMSE	AIC	BIC	LogLik
Dur–Sev	Ext. RLUF-type (BB7)	$\theta = 1.002, \delta = 7.689, a = 0.050, b = 3.690, c_1 = 10.0, c_2 = 0.783, m = 3.356, n = 0.906, \theta_2 = -7.973 \times 10^7$	0.578	-316.43	-299.40	167.22
Dur–Sev	Ext. RLUF-type (Gumbel)	$\theta = 1.990, a = 0.050, b = 1.966, c_1 = 7.342, c_2 = 1.207, m = 2.220, n = 1.064, \theta_2 = -1.404 \times 10^6$	0.578	-148.10	-132.97	82.05
Dur–Sev	Ext. RLUF-type (Clayton)	$\theta = 1.722, a = 0.050, b = 1.121, c_1 = 7.159, c_2 = 1.768, m = 2.191, n = 0.846, \theta_2 = -1.836 \times 10^6$	0.578	-142.96	-127.83	79.48
Dur–Sev	Ext. RLUF-type (Stud-t)	$\rho = 0.738, \nu = 100.0, a = 0.050, b = 1.586, c_1 = 6.866, c_2 = 1.463, m = 2.141, n = 1.041, \theta_2 = -1.126 \times 10^6$	0.578	-138.32	-121.30	78.16
Dur–Sev	Ext. RLUF-type (BB1)	$\theta = 1.140, \delta = 1.392, a = 0.050, b = 1.451, c_1 = 6.424, c_2 = 1.521, m = 2.063, n = 1.018, \theta_2 = -6.161 \times 10^5$	0.578	-125.96	-108.93	71.98
Dur–Sev	Gumbel	$\theta = 1.438$	0.208	-5.86	-3.97	3.93
Dur–Sev	Student-t	$\rho = 0.560, \nu = 100.0$	0.197	-5.52	-1.73	4.76
Dur–Sev	BB1	$\theta = 0.166, \delta = 1.379$	0.205	-4.07	-0.29	4.04
Dur–Sev	BB7	$\theta = 1.475, \delta = 0.377$	0.208	-3.58	0.21	3.79
Dur–Sev	Clayton	$\theta = 0.759$	0.212	-2.49	-0.60	2.25
Dur–Peak	Ext. RLUF-type (Clayton)	$\theta = 1.372, a = 0.050, b = 0.316, c_1 = 8.172, c_2 = 0.489, m = 2.347, n = 1.084, \theta_2 = -3.263 \times 10^6$	0.588	-155.29	-140.16	85.65
Dur–Peak	Ext. RLUF-type (BB1)	$\theta = 0.003, \delta = 1.004, a = 0.050, b = 0.639, c_1 = 7.148, c_2 = 0.996, m = 2.189, n = 0.937, \theta_2 = -1.607 \times 10^6$	0.588	-142.35	-125.32	80.17
Dur–Peak	Ext. RLUF-type (Stud-t)	$\rho = -0.564, \nu = 99.794, a = 0.050, b = 0.472, c_1 = 7.681, c_2 = 0.861, m = 2.273, n = 0.958, \theta_2 = -1.282 \times 10^6$	0.588	-134.77	-117.74	76.38
Dur–Peak	Ext. RLUF-type (BB7)	$\theta = 1.000, \delta = 0.805, a = 0.070, b = 0.918, c_1 = 6.460, c_2 = 1.107, m = 2.030, n = 0.967, \theta_2 = -3.725 \times 10^5$	0.588	-113.51	-96.48	65.75
Dur–Peak	Ext. RLUF-type (Gumbel)	$\theta = 1.351, a = 0.056, b = 0.511, c_1 = 4.456, c_2 = 0.584, m = 1.630, n = 2.026, \theta_2 = -4438.54$	0.587	-56.47	-41.33	36.23
Dur–Peak	Clayton	$\theta = 0.577$	0.212	-0.64	1.25	1.32
Dur–Peak	Gumbel	$\theta = 1.239$	0.215	-0.57	1.32	1.28
Dur–Peak	Student-t	$\rho = 0.416, \nu = 100.0$	0.204	0.20	3.98	1.90
Dur–Peak	BB1	$\theta = 0.331, \delta = 1.146$	0.208	0.77	4.55	1.62
Dur–Peak	BB7	$\theta = 1.173, \delta = 0.451$	0.210	0.96	4.74	1.52

Overall, extended RLUF-type copulas consistently outperform classical families across all provinces, demonstrating superior capability in modeling nonlinear, asymmetric, and tail-dependent structures. These selected models provide a robust foundation for subsequent bivariate flood risk and return period analyses.

3.3. **Spatial Distribution and Magnitude of Joint Return Periods of Flood Characteristics in Region XI.** Figures 5 and 6 present the spatial distribution of joint return periods for duration–peak and duration–severity combinations across Region XI. These maps were derived using the selected marginal distributions and optimal copula models, with spatial interpolation applied to capture regional flood risk continuity. It is important to note that the spatial return period maps presented in Figures 5 and 6 are derived using the joint (AND) return period framework, which quantifies the expected recurrence interval of compound flood events characterized by the simultaneous exceedance of specified thresholds in the considered hydrological variables.

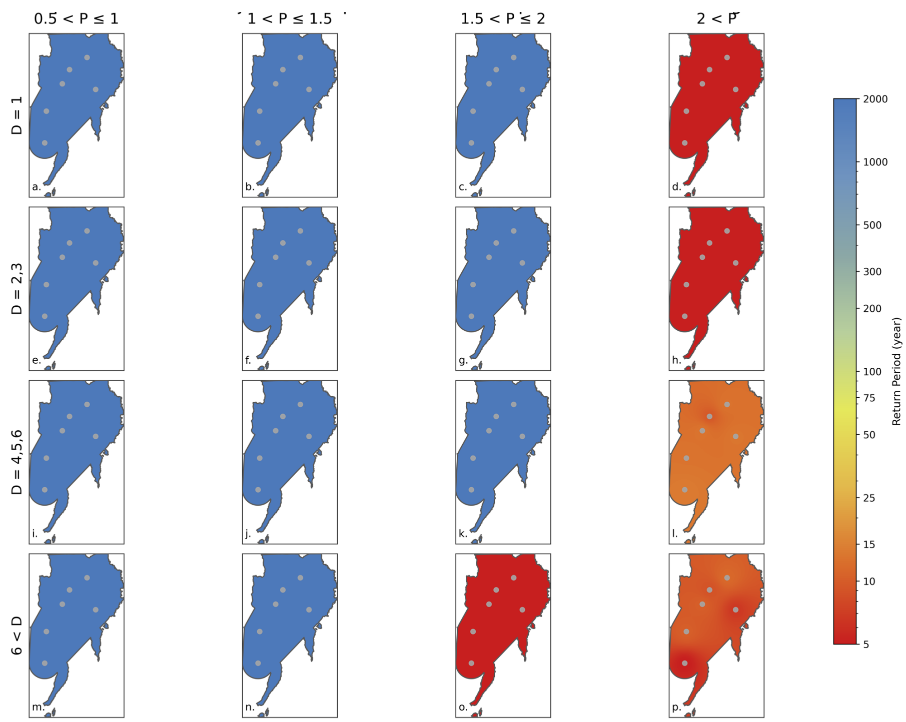

FIGURE 5. Spatial distribution of joint return period (years) for flood peak and duration across Region XI. Columns represent peak classes ($0.5 < P \leq 1, 1 < P \leq 1.5, 1.5 < P \leq 2$, and $P > 2$), while rows correspond to duration classes ($D = 1$, $D = 2$–3, $D = 4$–6, and $D > 6$). Warmer colors indicate shorter return periods (higher frequency), whereas cooler colors indicate longer return periods (lower frequency).

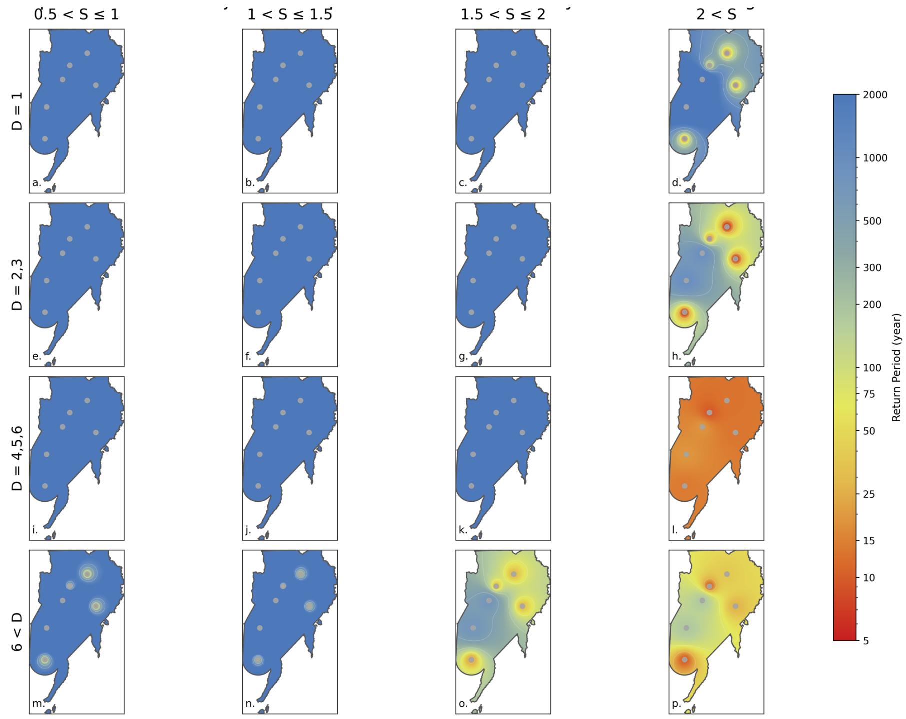

FIGURE 6. Spatial distribution of joint return period (years) for flood severity and duration across Region XI. Columns represent severity classes ($0.5 < S \leq 1$, $1 < S \leq 1.5$, $1.5 < S \leq 2$, and $S > 2$), while rows correspond to duration classes ($D = 1$, $D = 2$–3, $D = 4$–6, and $D > 6$). Warmer colors indicate more frequent events, while cooler colors denote rarer events.

3.3.1. *Spatial Dynamics of the Duration–Severity Relationship.* The joint return periods (T_{AND}) visualized in Figure 6 reveal significant spatial heterogeneity in flood hazard across the Davao Region. Analysis of the $S > 2$ magnitude class indicates a high frequency of high-severity events in Davao de Oro, Davao del Norte, Davao Occidental, and Davao Oriental, with T_{AND} values ranging from 2.6 to 4.8 years for short-to-moderate durations ($D \leq 3$). This identifies these provinces as regional hotspots for compound extremes, where high intensity coincides with rapid hydrological response.

Conversely, prolonged events ($D > 6$) exhibit a distinct risk profile. While return periods for long-duration floods are generally higher, moderate-to-high severity events remain hydrologically plausible in mountainous and coastal provinces (e.g., Davao de Oro and Davao Occidental), with T_{AND} values between 8.0 and 37.9 years. In contrast, urbanized zones like Davao City demonstrate greater stability for moderate severity classes ($S \leq 2$), suggesting a lower probability of compound duration-severity events compared to the region's more rugged topographies. These findings underscore a multi-modal hazard regime, necessitating localized design and early-warning thresholds that account for both high-intensity pulses and sustained inundation risks.

3.3.2. *Spatial Dynamics of the Duration–Peak Relationship.* The multivariate hazard profiles for the duration–peak relationship (Figure 5) indicate a pronounced susceptibility to high-magnitude discharge across the Davao Region. Joint return period (T_{AND}) analysis reveals that low-to-moderate peak classes ($P \leq 2$) are associated with extremely large recurrence intervals, whereas high-peak events ($P > 2$) exhibit significantly lower return periods, typically ranging from 2.6 to 4.8 years for short-to-moderate durations ($D \leq 3$). This highlights a regional regime dominated by frequent, high-intensity hydrological pulses.

Notably, elevated peak magnitudes persist as a significant hazard even during extended durations ($D \geq 4$). For the $2 < P$ class, return periods remain within the 8.8 to 13.9-year range across most stations, suggesting that sustained high-flow events are a critical component of the regional risk profile. In Davao Occidental, a unique shift occurs at $6 < D$, where the return periods for moderate-to-high peaks ($1 < P \leq 2$) drop to between 2.1 and 3.2 years, identifying this area as particularly vulnerable to prolonged, moderate-intensity inundation. These findings demonstrate that flood risk in the region is driven by a combination of rapid runoff generation and sustained hydrological response, necessitating infrastructure designs capable of mitigating both flash-flood peaks and persistent high-volume flows.

4. Summary and Conclusion

This study established a robust copula-based multivariate framework to characterize the complex flood regime of Region XI, Philippines, by integrating SPI-derived duration (D), peak (P), and severity (S). By transcending traditional univariate limitations, the research identified optimal marginal distributions, characterized nonlinear dependence structures, and quantified bivariate joint return periods (T_{AND}) critical for regional risk assessment.

Key findings indicate that flood characteristics in the region are governed by strongly skewed, heavy-tailed behaviors. The Lomax distribution consistently modeled duration, while the Generalized Gamma (and Fatigue Life in specific rugged topographies) and Beta Prime distributions provided the best fits for peak and severity, respectively. Dependence modeling revealed intricate, asymmetric relationships where extended RLUF-type copulas (specifically BB7, BB1, and Clayton) systematically outperformed classical Archimedean models in capturing the upper-tail dependencies inherent in compound extremes.

Spatial hazard mapping through joint return period analysis (T_{AND}) exposed a multi-modal risk landscape:

- **High-Intensity Pulses:** Provinces such as Davao de Oro and Davao Oriental are identified as hotspots for high-magnitude, short-duration events ($S > 2, P > 2$), with recurrence intervals as frequent as 2.6 to 4.8 years.

- **Topographic Vulnerability:** Mountainous and coastal zones exhibit non-negligible probabilities for prolonged inundations $(D > 6)$, with moderate-to-high severity events remaining hydrologically plausible.
- **Hydrological Regimes:** The results confirm that flood behavior in Region XI is driven by a synergy of rapid runoff generation and sustained moisture persistence, which univariate models fail to detect.

In conclusion, this framework provides a scientifically rigorous foundation for hydrological planning and disaster risk management in the Davao Region. By offering precise estimation of compound return periods, the study facilitates the design of hydraulic infrastructure that accounts for the simultaneous occurrence of critical flood parameters. Future research should prioritize higher-dimensional vine copula structures and the integration of nonstationary climatic covariates to further refine the predictive capacity of the model under a changing climate.

Acknowledgements. The author acknowledges the University of Southeastern Philippines for providing an enabling research environment and institutional support that made this study possible.

Conflicts of Interest. The author declares that there are no conflicts of interest regarding the publication of this paper.

References

[1] K. Aas, C. Czado, A. Frigessi, H. Bakken, Pair-Copula Constructions of Multiple Dependence, Insur. Math. Econ. 44 (2009), 182–198. https://doi.org/10.1016/j.insmatheco.2007.02.001.

[2] H. Akaike, A New Look at the Statistical Model Identification, IEEE Trans. Autom. Control 19 (1974), 716–723. https://doi.org/10.1109/TAC.1974.1100705.

[3] T.W. Anderson, D.A. Darling, Asymptotic Theory of Certain "Goodness of Fit" Criteria Based on Stochastic Processes, Ann. Math. Stat. 23 (1952), 193–212. https://doi.org/10.1214/aoms/1177729437.

[4] B.C. Arnold, Pareto Distribution, in: Wiley StatsRef: Statistics Reference Online, Wiley, 2015: pp. 1–10. https://doi.org/10.1002/9781118445112.stat01100.pub2.

[5] T. Bedford, R.M. Cooke, Vines—a New Graphical Model for Dependent Random Variables, Ann. Stat. 30 (2002), 1031–1068. https://doi.org/10.1214/aos/1031689016.

[6] B. Bobée, The Gamma Family and Derived Distributions Applied in Hydrology, Water Resources Publications, 1991.

[7] R. Chhikara, J.L. Folks, The Inverse Gaussian Distribution, CRC Press, 2024. https://doi.org/10.1201/9781003573746.

[8] J.V.B. Deluao, M.O. Macalos, J.P. Arcede, Construction of RLUF-Type Copula Generated by Rüschendorf Method to Model Time-Varying Dependency for Dengue R_{eff}, Precipitation and Temperature, Asia Pac. J. Math. 11 (2024), 105. https://doi.org/10.28924/APJM/11-105.

[9] Y. Feng, K.L. Brubaker, R.H. McCuen, New View of Flood Frequency Incorporating Duration, J. Hydrol. Eng. 22 (2017), 04017051. https://doi.org/10.1061/(ASCE)HE.1943-5584.0001573.

[10] C. Genest, A.-C. Favre, Everything You Always Wanted to Know about Copula Modeling but Were Afraid to Ask, J. Hydrol. Eng. 12 (2007), 347–368. https://doi.org/10.1061/(ASCE)1084-0699(2007)12:4(347).

[11] C. Genest, B. Rémillard, D. Beaudoin, Goodness-of-Fit Tests for Copulas: A Review and a Power Study, Insur. Math. Econ. 44 (2009), 199–213. https://doi.org/10.1016/j.insmatheco.2007.10.005.

[12] J. Kim, E.A. Sungur, T. Choi, T.Y. Heo, Generalized Bivariate Copulas and Their Properties, Model Assist. Stat. Appl. 6 (2011), 127–136. https://doi.org/10.3233/MAS-2011-0185.

[13] J.R.M. Hosking, Regional Frequency Analysis, Cambridge University Press, 1997.

[14] H. Joe, Dependence Modeling with Copulas, Chapman and Hall/CRC, 2014. https://doi.org/10.1201/b17116.

[15] N.L. Johnson, Systems of Frequency Curves Generated by Methods of Translation, Biometrika 36 (1949), 149. https://doi.org/10.2307/2332539.

[16] J. Kim, E.A. Sungur, T. Choi, T. Heo, Generalized Bivariate Copulas and Their Properties, Model Assist. Stat. Appl. 6 (2011), 127–136. https://doi.org/10.3233/MAS-2011-0185.

[17] C. Kleiber, S. Kotz, Statistical Size Distributions in Economics and Actuarial Sciences, Wiley, 2003. https://doi.org/10.1002/0471457175.

[18] M. Lang, T.B.M.J. Ouarda, B. Bobée, Towards Operational Guidelines for Over-Threshold Modeling, J. Hydrol. 225 (1999), 103–117. https://doi.org/10.1016/S0022-1694(99)00167-5.

[19] J.F. Lawless, Statistical Models and Methods for Lifetime Data, Wiley, 2003.

[20] V. Leiva, Birnbaum-Saunders Distribution, Elsevier, 2016.

[21] E. Limpert, W.A. Stahel, M. Abbt, Log-Normal Distributions across the Sciences: Keys and Clues, BioScience 51 (2001), 341. https://doi.org/10.1641/0006-3568(2001)051[0341:lndats]2.0.co;2.

[22] T.B. McKee, N.J. Doesken, J. Kleist, The Relationship of Drought Frequency and Duration to Time Scales, in: Proceedings of the 8th Conference on Applied Climatology, American Meteorological Society, pp. 179–184, 1993.

[23] T.B. McKee, N.J. Doesken, J. Kleist, Drought Monitoring with Multiple Time Scales, in: Proceedings of the 9th Conference on Applied Climatology, American Meteorological Society, pp. 233–236, 1995.

[24] A. Mishra, S. Mukherjee, B. Merz, V.P. Singh, D.B. Wright, et al., An Overview of Flood Concepts, Challenges, and Future Directions, J. Hydrol. Eng. 27 (2022), 03122001. https://doi.org/10.1061/(ASCE)HE.1943-5584.0002164.

[25] NASA, Prediction Of Worldwide Energy Resources, https://www.earthdata.nasa.gov/data/projects/power.

[26] R.B. Nelsen, An Introduction to Copulas, Springer, 2006. https://doi.org/10.1007/0-387-28678-0.

[27] J. Rodríguez-Lallena, A New Class of Bivariate Copulas, Stat. Probab. Lett. 66 (2004), 315–325. https://doi.org/10.1016/j.spl.2003.09.010.

[28] G. Salvadori, C. De Michele, Frequency Analysis via Copulas: Theoretical Aspects and Applications to Hydrological Events, Water Resour. Res. 40 (2004), 2004WR003133. https://doi.org/10.1029/2004WR003133.

[29] G. Salvadori, C. De Michele, N.T. Kottegoda, R. Rosso, Extremes in Nature: An Approach Using Copulas, Springer, 2007. https://doi.org/10.1007/1-4020-4415-1.

[30] G. Schwarz, Estimating the Dimension of a Model, Ann. Stat. 6 (1978), 461–464. https://doi.org/10.1214/aos/1176344136.

[31] R.A. Seiler, M. Hayes, L. Bressan, Using the Standardized Precipitation Index for Flood Risk Monitoring, Int. J. Climatol. 22 (2002), 1365–1376. https://doi.org/10.1002/joc.799.

[32] J.T. Shiau, Fitting Drought Duration and Severity with Two-Dimensional Copulas, Water Resour. Manag. 20 (2006), 795–815. https://doi.org/10.1007/s11269-005-9008-9.

[33] J.T. Shiau, H.Y. Wang, C.T. Tsai, Bivariate Frequency Analysis of Floods Using Copulas, J. Am. Water Resour. Assoc. 42 (2006), 1549–1564. https://doi.org/10.1111/j.1752-1688.2006.tb06020.x.

[34] E.W. Stacy, A Generalization of the Gamma Distribution, Ann. Math. Stat. 33 (1962), 1187–1192. https://doi.org/10.1214/aoms/1177704481.

[35] H.C.S. Thom, A Note on the Gamma Distribution, Mon. Weather Rev. 86 (1958), 117–122. https://doi.org/10.1175/1520-0493(1958)086<0117:ANOTGD>2.0.CO;2.

[36] S.M. Vicente-Serrano, S. Beguería, J.I. López-Moreno, A Multiscalar Drought Index Sensitive to Global Warming: The Standardized Precipitation Evapotranspiration Index, J. Clim. 23 (2010), 1696–1718. https://doi.org/10.1175/2009JCLI2909.1.

[37] World Meteorological Organization, Standardized Precipitation Index User Guide, World Meteorological Organization, 2012.

[38] V.M. Yevjevich, An Objective Approach to Definitions and Investigations of Continental Hydrologic Droughts, Colorado State University, 1967. http://hdl.handle.net/10217/61303.

[39] L. Zhang, V.P. Singh, Bivariate Flood Frequency Analysis Using the Copula Method, J. Hydrol. Eng. 11 (2006), 150–164. https://doi.org/10.1061/(ASCE)1084-0699(2006)11:2(150).